Anisotropic flow of identified particles in Pb-Pb collisions at √sNN=5.02 TeV
ALICE Collaboration

Anisotropic flow of identified particles in Pb-Pb collisions at $\sqrt{s}_{\mathrm{NN}} = 5.02\,\mathrm{TeV}$

ALICE

The ALICE collaboration

E-mail: ALICE-publications@cern.ch

ABSTRACT: The elliptic (v_2), triangular (v_3), and quadrangular (v_4) flow coefficients of $\pi^{\pm}$, $\mathrm{K}^{\pm}$, $\mathrm{p} + \overline{\mathrm{p}}$, $\Lambda + \overline{\Lambda}$, $\mathrm{K}_{\mathrm{S}}^0$, and the ϕ-meson are measured in Pb-Pb collisions at $\sqrt{s_{\mathrm{NN}}} = 5.02\,\mathrm{TeV}$. Results obtained with the scalar product method are reported for the rapidity range $|y| < 0.5$ as a function of transverse momentum, p_{T}, at different collision centrality intervals between 0–70%, including ultra-central (0–1%) collisions for $\pi^{\pm}$, $\mathrm{K}^{\pm}$, and $\mathrm{p} + \overline{\mathrm{p}}$. For $p_{\mathrm{T}} < 3\,\mathrm{GeV}/c$, the flow coefficients exhibit a particle mass dependence. At intermediate transverse momenta ($3 < p_{\mathrm{T}} < 8$–$10\,\mathrm{GeV}/c$), particles show an approximate grouping according to their type (i.e., mesons and baryons). The ϕ-meson v_2, which tests both particle mass dependence and type scaling, follows $\mathrm{p} + \overline{\mathrm{p}}$ v_2 at low p_{T} and $\pi^{\pm}$ v_2 at intermediate p_{T}. The evolution of the shape of $v_{\mathrm{n}}(p_{\mathrm{T}})$ as a function of centrality and harmonic number n is studied for the various particle species. Flow coefficients of $\pi^{\pm}$, $\mathrm{K}^{\pm}$, and $\mathrm{p} + \overline{\mathrm{p}}$ for $p_{\mathrm{T}} < 3\,\mathrm{GeV}/c$ are compared to iEBE-VISHNU and MUSIC hydrodynamical calculations coupled to a hadronic cascade model (UrQMD). The iEBE-VISHNU calculations describe the results fairly well for $p_{\mathrm{T}} < 2.5\,\mathrm{GeV}/c$, while MUSIC calculations reproduce the measurements for $p_{\mathrm{T}} < 1\,\mathrm{GeV}/c$. A comparison to v_{n} coefficients measured in Pb-Pb collisions at $\sqrt{s_{\mathrm{NN}}} = 2.76\,\mathrm{TeV}$ is also provided.

Contents

1 Introduction

Ultra-relativistic heavy-ion collisions are used to study the properties of the quark-gluon plasma (QGP), a state of deconfined quarks and gluons expected at high temperatures or baryon densities [1]. Measurements of anisotropies in particle azimuthal distributions relative to the collision symmetry planes at the Relativistic Heavy Ion Collider (RHIC) [2–5] and the Large Hadron Collider (LHC) [6–8] have shown that the produced hot and dense matter behaves as a strongly-interacting QGP. Comparisons to predictions from hydrodynamic models indicate that the QGP has a shear viscosity to entropy density ratio (η/s) close to the theoretical lower limit from the anti-de Sitter/conformal field theory (AdS/CFT) correspondence of $1/4\pi$ for $\hbar = k_B = 1$ [9].

Azimuthal anisotropies in particle production relative to the collision symmetry planes, often referred to as anisotropic flow, arise from the asymmetry in the initial geometry of the collision combined with the initial inhomogeneities of the system's energy density [10]. Anisotropic flow depends on the equation of state and transport coefficients of the system,

such as η/s and bulk viscosity to entropy density ratio (ζ/s). Its magnitude is quantified via the coefficients v_n in a Fourier decomposition of the particle azimuthal distribution [11]

$$E\frac{\mathrm{d}^3N}{\mathrm{d}p^3} = \frac{1}{2\pi}\frac{\mathrm{d}^2N}{p_T\mathrm{d}p_T\mathrm{d}y}\left(1 + 2\sum_{n=1}^{\infty}v_n\cos[n(\varphi - \Psi_n)]\right), \qquad (1.1)$$

where E is the energy, p the momentum, p_T the transverse momentum, φ the azimuthal angle, η the pseudorapidity of the particle, and Ψ_n the n-th harmonic symmetry plane angle. The second order flow coefficient v_2, called *elliptic flow*, is the largest contribution to the asymmetry of non-central collisions because of the almond-like geometry of the overlap region between the colliding nuclei in the plane perpendicular to the beam direction. The third-order flow coefficient v_3, named *triangular flow*, is generated by fluctuations in the initial distribution of nucleons and gluons in the overlap region [12–15]. The fourth-order flow coefficient v_4, called *quandrangular flow*, is generated both by initial geometry, fluctuations, and is in addition sensitive to the non-linear hydrodynamic response of the medium [16, 17]. It has been shown that higher-order flow coefficients are more sensitive to η/s than v_2 [18, 19].

In addition to probing η/s and ζ/s, anisotropic flow constrains the initial spatial density (e.g. energy and entropy density), freeze-out conditions of the system, and particle production mechanisms in different p_T regions. Stronger constraints are achieved by studying anisotropic flow of identified particles. To guide interpretation of the results in the context of these processes, three kinematic 'regions of interest' are defined in the p_T-differential v_n measurements, $v_n(p_T)$. For $p_T \lesssim 3$ GeV/c, anisotropic flow is a remnant of the collective dynamics during the hydrodynamic expansion of the system. The interplay between the isotropic expansion (radial flow) and anisotropic flow leads to a characteristic mass ordering of $v_n(p_T)$ [20–28], meaning that heavier particles have smaller $v_n(p_T)$. At intermediate p_T $(3 \lesssim p_T \lesssim 8$ GeV/$c)$, the values of v_n for different particles tend to separate mesons and baryons [27–33]. The flow of baryons is larger than that of mesons in this p_T range, supporting the hypothesis of hadronization through quark coalescence [34], where it is assumed that the invariant spectrum of produced particles is proportional to the product of the spectra of their constituents [35, 36]. However, the scaling only holds approximately at RHIC [32] and at the level of $\pm 20\%$ in Pb-Pb collisions at $\sqrt{s_{NN}} = 2.76$ TeV [27, 28]. This behaviour is also qualitatively consistent with a scenario in which particle production includes interactions of jet fragments with bulk matter [37, 38]. For $p_T \gtrsim 8$ GeV/c, anisotropic flow is generated when hard partons that propagate through the system lose energy via (multiple) scattering and gluon radiation [39, 40], resulting in v_n that remain non-zero up to very high p_T [41–44].

Anisotropic flow of identified particles is an important observable when studying the characteristics of the QGP. However, since particles can scatter and be regenerated in between the chemical and kinetic freeze-out of a collision (the *hadronic phase*), information about the QGP phase imprinted in $v_n(p_T)$ can be altered by late-stage interactions and resonance decays, which can affect both v_n and $\langle p_T \rangle$ [45], leading to a deviation in mass ordering in $v_n(p_T)$ at low p_T [46]. The ϕ-meson has been suggested as a particularly sensitive probe of the early collision phase as its production rate via regeneration in the hadronic

phase is negligible [47] and it is theorized to have a low hadronic cross section [48–50], making it insensitive to the dissipative effects of the hadronic phase of the collision (although it should be noted that there is no consensus on the exact value of the cross section between the ϕ-meson and nucleons in heavy-ion collisions [51–54]). Recent experimental studies [27, 55, 56] suggest that the ϕ-meson may be more sensitive to the hadronic phase than anticipated.

In this article, we present measurements of p_{T}-differential elliptic, triangular, and quadrangular flow coefficients of $\pi^{\pm}$, $K^{\pm}$, $p+\overline{p}$, $\Lambda+\overline{\Lambda}$, K_S^0, and the ϕ-meson in Pb-Pb collisions at $\sqrt{s_{\mathrm{NN}}} = 5.02\,\mathrm{TeV}$, extending greatly, and improving in precision upon, the previous measurements of identified particle v_{n} in Pb-Pb collisions at $\sqrt{s_{\mathrm{NN}}} = 2.76\,\mathrm{TeV}$ as carried out by ALICE [27, 28, 33]. The results are reported for a wide range of particle transverse momenta within the rapidity range $|y| < 0.5$ at different collision centralities between 0–70% range. To isolate the fraction of anisotropic flow that is generated by initial-state fluctuations rather than geometry, the flow coefficients are also studied in ultra-central collisions (0–1% collision centrality). Centrality estimates the degree of overlap between the two colliding nuclei and is expressed as percentiles of the inelastic hadronic cross section, with low percentage values corresponding to head-on collisions. The measurements are performed using the scalar product method [57–59] with a (pseudo-)rapidity gap of $|\Delta\eta| > 2.0$ between the identified particles under study and the charged reference particles. The flow coefficients are measured separately for particles and anti-particles and are found to be compatible within the statistical uncertainties for most p_{T} and centrality intervals. Any residual differences are included in the systematic uncertainties, and v_{n} denotes the average between results for particles and anti-particles.

This paper is organized as follows. Analysis details, particle identification, reconstruction methods, and flow measurement techniques are outlined in section 2. The evaluation of systematic uncertainties is discussed in section 3. The flow coefficients of $\pi^{\pm}$, $K^{\pm}$, $p+\overline{p}$ (v_2, v_3, and v_4), $\Lambda+\overline{\Lambda}$, K_S^0 (v_2 and v_3), and the ϕ-meson (v_2) are reported and compared to model calculations in section 4. Finally, the results are summarized in section 5.

2 Experimental setup and data analysis

ALICE [60–62] is a dedicated heavy-ion experiment at the LHC optimized to study the properties of strongly interacting matter produced in heavy-ion collisions. A full overview of the detector layout and its performance can be found in [62, 63]. The main subsystems used in this analysis are the Inner Tracking System (ITS) [64], Time Projection Chamber (TPC) [65], Time Of Flight detector (TOF) [66], and V0 [67]. The ITS, TPC, and TOF detectors cover full azimuth within pseudorapidity range $|\eta| < 0.9$ and lie within a homogeneous magnetic field of up to 0.5 T. The ITS consists of six layers of silicon detectors used for tracking and vertex reconstruction. The TPC is the main tracking detector and is also used to identify particles via specific ionization energy loss, $\mathrm{d}E/\mathrm{d}x$. The TOF in conjunction with the timing information from the T0 detector [68] provide particle identification based on flight time. The T0 is made up of two arrays of Cherenkov counters T0C and T0A, located at $-3.3 < \eta < -3.0$ and $4.5 < \eta < 4.9$, respectively. Two scintillator arrays

(V0), which cover the pseudorapidity ranges $-3.7 < \eta < -1.7$ (V0C) and $2.8 < \eta < 5.1$ (V0A), are used for triggering, event selection, and the determination of centrality [69] and $\mathbf{Q}_n$-vectors (see section 2.5). Both V0 detectors are segmented in four rings in the radial direction with each ring divided into eight sectors in the azimuthal direction. In addition, two tungsten-quartz neutron Zero Degree Calorimeters (ZDCs), installed 112.5 meters from the interaction point on each side, are used for event selection.

2.1 Event and track selection

The data sample recorded by ALICE during the 2015 LHC Pb-Pb run at $\sqrt{s_{NN}} = 5.02\,\mathrm{TeV}$ is used for this analysis. The minimum-bias trigger requires signals in both V0A and V0C detectors. An offline event selection is applied to remove beam-induced background (i.e. beam-gas events) and pileup events. The former is rejected utilizing the V0 and ZDC timing information. The remaining contribution of such interactions is found to be smaller than 0.02% [63]. Pileup events, which constitute about 0.25% of the recorded sample, are removed by comparing multiplicity estimates from the V0 detector to those of tracking detectors at mid-rapidity, exploiting the difference in readout times between the systems. The fraction of pileup events left after applying the dedicated pileup removal criteria is found to be negligible. The primary vertex position is determined from tracks reconstructed in the ITS and TPC as described in ref. [63]. Only events with a primary vertex position within ± 10 cm from the nominal interaction point along the beam direction are used in the analysis. Approximately 67×10^6 Pb-Pb events in the 0–70% centrality interval pass these selection criteria. Centrality is estimated from the energy deposition measured in the V0 detector [69].

Charged-particle tracks, used to measure the v_n of $\pi^\pm$, $K^\pm$, p+$\overline{\mathrm{p}}$ and the ϕ-meson, are reconstructed using the ITS and TPC within $|\eta| < 0.8$ and $0.5 < p_T < 16.0\,\mathrm{GeV}/c$ with a track-momentum resolution better than 4% for the considered range [63]. Additional quality criteria are used to reduce the contamination from secondary charged particles (i.e., particles originating from weak decays, γ-conversions, and secondary hadronic interactions in the detector material) and fake tracks (random associations of space points). Only tracks with at least 70 space points, out of a maximum of 159, with a χ^2 per degree-of-freedom for the track fit lower than 2, are accepted. Moreover, each track is required to cross at least 70 TPC pad rows and to be reconstructed from at least 80% of the number of expected TPC space points, in addition to having at least one hit in the two innermost layers of the ITS. Furthermore, tracks with a distance of closest approach (DCA) to the reconstructed event vertex smaller than 2 cm in the longitudinal direction (z) and $(0.0105 + 0.0350\,(p_T\,c/\mathrm{GeV})^{-1.1})$ cm in the transverse plane (xy) are selected. Relevant selection criteria for tracks used for the reconstruction of K_S^0 and $\Lambda+\overline{\Lambda}$ are given in section 2.3.

2.2 Identification of $\pi^\pm$, $K^\pm$ and p+$\overline{\mathrm{p}}$

Particle identification is performed using the specific ionization energy loss, dE/dx, measured in the TPC and the time of flight obtained from the TOF. A truncated-mean procedure is used to estimate the dE/dx (where the 40% highest-charge clusters are discarded), which yields a dE/dx resolution around 6.5% in the 0–5% centrality class [63]. At least 70

clusters are used for the dE/dx estimation. The TOF measures the time that a particle needs to travel from the primary vertex to the detector itself with a time resolution of ≈ 80 ps [63]. The start time for the TOF measurement is provided by the T0 detector or from a combinatorial algorithm which uses the particle arrival times at the TOF detector itself [63, 66].

Expressing the difference between the expected dE/dx and the time of flight for $\pi^{\pm}$, $K^{\pm}$ and p+$\overline{p}$, and the measured signals in both TPC and TOF, in units of the standard deviations from the most probable value for both detectors (nσ_{TPC}, nσ_{TOF}), and applying a selection on the number of accepted nσ, allows for particle identification on a track-by-track basis. The TPC dE/dx of different particle species are separated by at least 4σ for $p_T < 0.7$ GeV/c, while in the relativistic rise region of the dE/dx ($p_T > 2$ GeV/c) particle identification is still possible but only on a statistical basis [63]. The TOF detector provides 3σ separation between $\pi^{\pm}$ and $K^{\pm}$ for $p_T < 2.5$ GeV/c, and between $K^{\pm}$ and p+$\overline{p}$ for $p_T < 4$ GeV/c [63].

The information from the TPC and TOF is combined using a quadratic sum n$\sigma_{PID} = \sqrt{n\sigma_{TPC}^2 + n\sigma_{TOF}^2}$ for $0.5 < p_T \leq 4$ GeV/c. Particles are selected by requiring n$\sigma_{PID} < 3$ for each species. The smallest nσ_{PID} is used to assign the identity when the selection criterion is fulfilled by more than one species. When measuring p+$\overline{p}$ $v_n(p_T)$, only $\overline{p}$ are considered for $p_T < 2$ GeV/c to exclude secondary protons from detector material. At high transverse momenta ($p_T > 4$ GeV/c), $K^{\pm}$ cannot reliably be identified. Identification of $\pi^{\pm}$ and p+$\overline{p}$ for $p_T > 4$ GeV/c is done utilizing the TPC dE/dx signal only. Pions (protons) are selected from the upper (lower) part of the expected pion (proton) dE/dx distribution. For example, proton selection typically varies in the range from 0 to $-3\sigma_{TPC}$ or from $-1.5\sigma_{TPC}$ to $-4.5\sigma_{TPC}$ depending on the momentum.

Secondary contamination from weak decays, studied using the procedure outlined in [70], decreases from about 30% to 5% for p+$\overline{p}$ in the p_T range 0.7–4.0 GeV/c and from about 5% to 0.5% for $\pi^{\pm}$ in the p_T range 0.5–4.0 GeV/c, while it is negligible for $K^{\pm}$. The v_n coefficients are not corrected for these contaminations; their effect on v_n is at maximum $\approx 8\%$, for p + $\overline{p}$ v_2 at $p_T < 1$ GeV/c for central collisions, and negligible for $K^{\pm}$, $\pi^{\pm}$ v_n. The contamination from other particle species is below 3% and 20% at $p_T > 4.0$ GeV/c for $\pi^{\pm}$ and p+$\overline{p}$, respectively, and contamination from fake tracks is negligible. The v_n results are reported for $0.5 < p_T < 16.0(12.0, 6.0)$ GeV/c for $\pi^{\pm}$ v_2 (v_3, v_4), $0.7 < p_T < 16.0(12.0, 6.0)$ GeV/c for p+$\overline{p}$ v_2 (v_3, v_4), and $0.5 < p_T < 4.0$ GeV/c for $K^{\pm}$ v_n, all within $|y| < 0.5$.

2.3 Reconstruction of K_S^0 and $\Lambda + \overline{\Lambda}$

The K_S^0 and $\Lambda + \overline{\Lambda}$ are reconstructed in the $K_S^0 \rightarrow \pi^+ + \pi^-$ and $\Lambda \rightarrow p + \pi^-$ ($\overline{\Lambda} \rightarrow \overline{p} + \pi^+$) channels with branching ratios of 69.2% [71] and 63.9% [71] respectively. Reconstruction of K_S^0 and $\Lambda + \overline{\Lambda}$ is based on identifying secondary vertices from which two oppositely-charged particles originate, called V^{0}s. Topological selection criteria pertaining to the shape of the V^0 decay can be imposed, as well as requirements on the species identity of the decay products (called *daughter particles*).

The V^0 candidates are selected to have an invariant mass between 0.4 and 0.6 GeV/c^2 and 1.07 and 1.17 GeV/c^2 for K$_S^0$ and $\Lambda+\overline{\Lambda}$, respectively. The invariant mass of the V^0 is calculated based on the assumption that the daughter particles are either a $\pi^+\pi^-$ pair, or a pπ^- ($\overline{p}\pi^+$) pair. The daughter particles have been identified over the entire p_T range using the TPC following the nσ approach detailed in section 2.2 ($|n\sigma_{TPC}| < 3$). The daughter tracks were reconstructed within $|\eta| < 0.8$, while the criteria on the number of TPC space points, the χ^2 per TPC space point per degree-of-freedom, the number of crossed TPC pad rows, and the percentage of the expected TPC space points used to reconstruct a track are identical to those applied for primary particles. In addition, the minimum DCA of daughter tracks to the primary vertex is 0.1 cm. Furthermore, the maximum DCA of daughter tracks to the secondary vertex is 0.5 cm to ensure that they are products of the same decay.

To reject secondary vertices arising from decays into more than two particles, the cosine of the pointing angle θ_p is required to be larger than 0.998. This angle is defined as the angle between the momentum-vector of the V^0 assessed at its decay position and the line connecting the V^0 decay vertex to the primary vertex and has to be close to 0 as a result of momentum conservation. In addition, the V^0 candidates are only accepted when they are produced at a distance between 5 and 100 cm from the nominal primary vertex in the radial direction. The lower value is chosen to avoid any bias from the efficiency loss when secondary tracks are being wrongly matched to clusters in the first layer of the ITS. To assess the systematic uncertainty related to contaminations from $\Lambda+\overline{\Lambda}$ and electron-positron pairs coming from γ-conversions to the K$_S^0$ sample, a selection in the Armenteros-Podolanski variables [72] is applied for the K$_S^0$ candidates, rejecting ones with $q \leq |\alpha|/5$. Here q is the momentum projection of the positively charged daughter track in the plane perpendicular to the V^0 momentum and $\alpha = (p_L^+ - p_L^-)/(p_L^+ + p_L^-)$, with $p_L^\pm$ the projection of the positive or negative daughter tracks' momentum onto the momentum of the V^0.

To obtain the p_T-differential yield of K$_S^0$ and $\Lambda+\overline{\Lambda}$ (which, together with background yields, are used for the v_n extraction cf. eq. (2.3)), invariant mass distributions at various p_T intervals are parametrized as a sum of a Gaussian distribution and a second-order polynomial function. The latter is introduced to account for residual contaminations (*background yield*) that are present in the K$_S^0$ and $\Lambda+\overline{\Lambda}$ signals after the topological and daughter track selections. The K$_S^0$ and $\Lambda+\overline{\Lambda}$ yields are extracted by integration of the Gaussian distribution. Obtained yields have not been corrected for feed-down from higher mass baryons ($\Xi^\pm$, $\Omega^\pm$) as earlier studies have shown that these have a negligible effect on the measured v_n [27]. The $v_n(p_T)$ results are reported within $|y| < 0.5$ and $0.5 < p_T < 10$ GeV/c for K$_S^0$ and $0.8 < p_T < 10$ GeV/c for $\Lambda+\overline{\Lambda}$.

2.4 Reconstruction of ϕ-mesons

The ϕ-meson is reconstructed in the $\phi \rightarrow$ K$^+$+K$^-$ channel with a branching ratio of 48.9% [71]. Its reconstruction proceeds by first identifying all primary K$^\pm$ tracks in an event, following the procedure for primary charged K$^\pm$ outlined in section 2.2. The K$^\pm$ identification criterion n$\sigma_{PID} < 3$ is chosen as it improves the significance of the ϕ-meson yield, while retaining a sufficient reconstruction efficiency. The vector sums of all pos-

sible $K^{\pm}$ pairs are called ϕ-meson *candidates*, the yield of which is obtained as function of invariant mass $M_{K^+K^-}$ in various p_T intervals. The p_T-differential ϕ-meson yield is obtained by first subtracting a *background* yield from the candidate yield. This background yield is estimated using an event-mixing technique [73], in which $K^{\pm}$ from different collisions are paired into background tracks, and is normalized to the candidate yield for $1.04 < M_{K^+K^-} < 1.09\,\mathrm{GeV}/c^2$. Collisions with similar characteristics (vertex position, centrality) are used for this mixing. To obtain the p_T-differential yield of ϕ-mesons, the invariant mass distributions of the candidate yield is, after the aforementioned subtraction, parametrized as a sum of a Breit-Wigner distribution and a second-order polynomial function, the latter introduced to account for residual contaminations. The ϕ-meson yields are extracted by integration of the Breit-Wigner distribution and, together with background yields, used for the v_n extraction (see eq. (2.3)). The $v_2(p_T)$ results are reported for $0.9 < p_T < 6.5\,\mathrm{GeV}/c$ within $|y| < 0.5$.

2.5 Flow analysis techniques

The flow coefficients v_n are measured using the scalar product method [57–59], written as

$$v_n\{\mathrm{SP}\} = \langle\langle \mathbf{u}_{n,k}\mathbf{Q}_n^* \rangle\rangle \Big/ \sqrt{\frac{\langle \mathbf{Q}_n\mathbf{Q}_n^{A*} \rangle \langle \mathbf{Q}_n\mathbf{Q}_n^{B*} \rangle}{\langle \mathbf{Q}_n^A\mathbf{Q}_n^{B*} \rangle}}, \tag{2.1}$$

where $\mathbf{u}_{n,k} = \exp(in\varphi_k)$ is the unit flow vector of the particle of interest k with azimuthal angle φ_k, $\mathbf{Q}_n$ is the event flow vector, and n is the harmonic number. Brackets $\langle \cdots \rangle$ denote an average over all events, the double brackets $\langle\langle \cdots \rangle\rangle$ an average over all particles in all events, and $*$ the complex conjugate.

The vector $\mathbf{Q}_n$ is calculated from the azimuthal distribution of the energy deposition measured in the V0A. Its x and y components are given by

$$Q_{n,x} = \sum_j w_j \cos(n\varphi_j), \; Q_{n,y} = \sum_j w_j \sin(n\varphi_j), \tag{2.2}$$

where the sum runs over the 32 channels j of the V0A detector, φ_j is the azimuthal angle of channel j defined by the geometric center, and w_j is the amplitude measured in channel j. The vectors $\mathbf{Q}_n^A$ and $\mathbf{Q}_n^B$ are determined from the azimuthal distribution of the energy deposition measured in the V0C and the azimuthal distribution of the tracks reconstructed in the ITS and TPC, respectively. The amplitude measured in each channel of the V0C (32 channels as for the V0A) is used as weight in the case of $\mathbf{Q}_n^A$, while unity weights are applied for $\mathbf{Q}_n^B$. Tracks used for $\mathbf{Q}_n^B$ are selected following the procedure for primary charged tracks outlined in section 2.1 for $0.2 < p_T < 5.0$ GeV/c. In order to account for a non-uniform detector response, the components of the $\mathbf{Q}_n$ and $\mathbf{Q}_n^A$ vectors are recalibrated using a recentering procedure (i.e. subtraction of the $\mathbf{Q}_n$-vector averaged over many events from the $\mathbf{Q}_n$-vector of each event) [74]. The large gap in pseudorapidity between $\mathbf{u}_{n,k}$ and $\mathbf{Q}_n$ ($|\Delta\eta| > 2.0$) greatly suppresses short-range correlations unrelated to the azimuthal asymmetry in the initial geometry, commonly referred to as 'non-flow'. These correlations largely come from the inter-jet correlations and resonance decays.
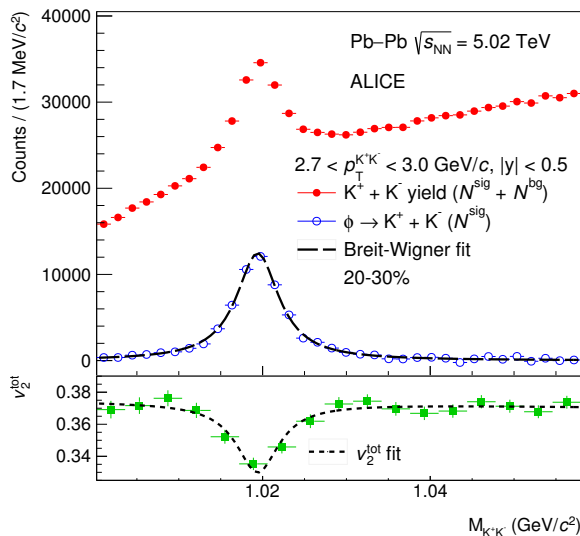
Figure 1. (Colour online) Illustration of reconstruction and v_2 measurement for the ϕ-meson. The reconstruction of the ϕ-meson and extraction of N^{sig} and N^{bg} are shown in the upper panel. A fit of eq. (2.3) to data is presented in the lower panel.

The v_{n} of the $\mathrm{K^0_S}$, $\Lambda+\overline{\Lambda}$, and ϕ-meson cannot directly be measured using eq. (2.1) as $\mathrm{K^0_S}$, $\Lambda+\overline{\Lambda}$ and the ϕ-meson cannot be identified on a particle-by-particle basis. Therefore, the v_n^{tot} of $\mathrm{V^0}$s and ϕ-meson candidates is measured as function of both invariant mass, $\mathrm{M_{d^+d^-}}$, and candidate p_{T}. This v_n^{tot} can be written [75] as the weighted sum of $v_{\mathrm{n}}(p_{\mathrm{T}})$ of the particle of interest, v_n^{sig}, and that of background tracks, $v_n^{\mathrm{bg}}(\mathrm{M_{d^+d^-}})$, as

$$v_{\mathrm{n}}^{\mathrm{tot}}(\mathrm{M_{d^+d^-}}) = v_{\mathrm{n}}^{\mathrm{sig}}\frac{N^{\mathrm{sig}}}{N^{\mathrm{sig}} + N^{\mathrm{bg}}}(\mathrm{M_{d^+d^-}}) + v_{\mathrm{n}}^{\mathrm{bg}}(\mathrm{M_{d^+d^-}})\frac{N^{\mathrm{bg}}}{N^{\mathrm{sig}} + N^{\mathrm{bg}}}(\mathrm{M_{d^+d^-}}), \qquad (2.3)$$

where *signal* and *background* yields N^{sig} and N^{bg} are obtained for each p_{T} interval from the $\mathrm{K^0_S}$, $\Lambda+\overline{\Lambda}$ and ϕ-meson reconstruction procedures outlined in sections 2.3 and 2.4. The formalism of eq. (2.1) is used to measure $v_{\mathrm{n}}^{\mathrm{tot}}(\mathrm{M_{d^+d^-}})$, $v_{\mathrm{n}}^{\mathrm{sig}}$ is obtained by parametrizing $v_{\mathrm{n}}^{\mathrm{bg}}(\mathrm{M_{d^+d^-}})$ as a second-order polynomial function and fitting eq. (2.3) to the data. Figure 1 illustrates this procedure for the ϕ-meson, showing the invariant mass spectrum of the ϕ-meson in the upper panel, and a fit of eq. (2.3) to $v_2^{\mathrm{tot}}(\mathrm{M_{d^+d^-}})$ data in the lower panel.

3 Systematic uncertainties

The systematic uncertainties on v_{n} fall into the following categories: those arising from event selection, those arising from charged particle tracking, uncertainties in particle identification, uncertainties in $\mathrm{V^0}$ finding, and those coming from the extraction of $v_{\mathrm{n}}(p_{\mathrm{T}})$.

For $p_{\mathrm{T}} \leq 4\,\mathrm{GeV}/c$, a p_{T}-dependent systematic uncertainty is assigned to v_2, v_3, and v_4 of $\pi^{\pm}$, $\mathrm{K^{\pm}}$, $\mathrm{p+\overline{p}}$, $\Lambda+\overline{\Lambda}$, $\mathrm{K^0_S}$ and the ϕ-meson. Per measured point, the difference between the nominal measurement and a variation on the nominal measurement is calculated. If this difference between the nominal data point and the systematic variation is significant (where significance is evaluated based on the recommendations in [76]), it is considered to

be a systematic uncertainty. When various checks are performed to quantify the effect of one systematic uncertainty (e.g. using three different centrality estimators to estimate the uncertainty in centrality determination), the maximum significant deviation that is found between the nominal measurement and the systematic variations is assigned as a systematic uncertainty. For each particle species, a p_T-independent average uncertainty is reported for $p_T > 4$ GeV/c in order to suppress sensitivity to statistical fluctuations. The uncertainty is obtained by fitting a zeroth-order polynomial to the significant p_T-dependent relative uncertainties.

The systematic uncertainties are evaluated (if applicable) for each particle species, $v_n(p_T)$ and centrality intervals. A quadratic sum of the systematic uncertainties from the independent sources is reported as final systematic uncertainty on the measurements. An overview of the magnitude of the relative systematic uncertainties per particle species is given in tables 1, 2, and 3 for v_2, v_3, and v_4, respectively.

Event selection. The nominal event selection criteria and centrality determination are discussed in section 2.1. Event selection criteria are varied by (i) changing the default centrality estimator from energy deposition in the V0 scintillator to either an estimate based on the number of hits in the first or second layer of the ITS; (ii) performing the v_n analysis of $\pi^\pm$, K$^\pm$, and p+$\overline{\text{p}}$ in 1% wide centrality intervals to test the effect of multiplicity fluctuations (a test not possible for K$_S^0$, $\Lambda+\overline{\Lambda}$ v_3); (iii) not rejecting events with tracks caused by pileup or imposing a stricter than default pileup rejection by requiring a tighter correlation between the V0 and central barrel multiplicities; (iv) requiring the reconstructed primary vertex of a collision to lie alternatively within ±12 cm and ±5 cm from the nominal interaction point along the beam axis; (v) analyzing events recorded under different magnetic field polarities independently; (v) analyzing events recorded at different collision rates independently.

Charged particle tracking. The nominal charged particle track selection criteria are outlined in section 2.1. Charged particle track selection criteria are varied by (i) requiring the third layer of the ITS to be part of the track reconstruction rather than the first two layers only; (ii) using only tracks that have at least three hits per track in the ITS, complemented by tracks without hits in the first two layers of the ITS (in which case the primary interaction vertex is used as an additional constraint for the momentum determination); (iii) changing the requirement on the minimum number of TPC space points that are used in the reconstruction from 70 to 60, 80, and 90; (iv) an additional systematic uncertainty is evaluated combining the following checks of the track quality: rejecting tracks that are reconstructed close to the sector boundaries of the TPC to which the sensitive pad rows do not extend, varying the minimum number of crossed TPC pad rows from 70 to 120, and requesting at least 90% instead of 80% of the expected TPC space points to reconstruct a track. Variations (i) and (ii) are referred to as *tracking mode* in tables 1, 2, and 3.

Particle identification. The nominal particle identification approach for $\pi^\pm$, K$^\pm$, and p+$\overline{\text{p}}$ is outlined in section 2.2. Particle identification criteria are varied by (i) changing the minimum number of clusters in the TPC that are used to estimate the dE/dx from 70 to 60, 80, and 90; (ii) rejecting tracks that satisfy the particle identification criterion for

Error source	$\pi^{\pm}$	$K^{\pm}$	$p+\bar{p}$	K^0_S	$\Lambda+\overline{\Lambda}$	ϕ
Vertex position	0–1%	0–1%	0–2%	0–2%	0–4%	1–6%
1% wide centrality intervals	0–3%	0–4%	0–4%			
Centrality estimator	0–3%	0–2%	0–3%	0–4%	0–5%	1–5%
Magnetic field polarity	0–2%	0–1%	0–2%	0–3%	0–3%	1–3%
Interaction rate	0–2%	0–1%	1–2%	*negl*	*negl*	*negl*
Pileup rejection	0–1%	0–1%	0–2%	0–1%	0–2%	0–1%
Tracking mode	0–4%	0–8%	0–10%			0–5%
Number of TPC space points	0–2%	0–2%	0–2%	0–4%	0–2%	*negl*
Track quality	0–3%	0–2%	0–3%	0–4%	0–3%	*negl*
Particle identification purity	0–5%	0–7%	0–5%	0–3%	0–8%	0–6%
Number of TPC clusters used for dE/dx	0–6%	0–5%	0–5%	0–5%	0%	*negl*
Exclusive particle identification	0–2%	0–3%	0–3%			
Decay vertex (radial position)				0–10%	0–11%	
Armenteros-Podolanski variables				0–2%		
DCA decay products to primary vertex				0–3%	0–5%	
DCA between decay products				0–2%	0–7%	
Pointing angle $\cos\theta_{\mathrm{p}}$				0–4%	0–9%	
Minimum p_{T} of daughter tracks				0–4%	0–5%	
Peak shape				*negl*	*negl*	*negl*
Residual background in yield				*negl*	*negl*	*negl*
Event mixing						1–3%
Positive and negative rapidities	0–3%	0–2%	0–2%	0–4%	0–7%	*negl*
Opposite charges	0–2%	0–2%	0–2%			
Channel removal from V0A	0–5%	0–5%	0–8%	0–3%	0–5%	0–4%
v_{n} from V0A or V0C	0–2%	0–2%	0–2%	*negl*	*negl*	*negl*
$v_{\mathrm{n}}^{\mathrm{bg}}$ parametrization				*negl*	*negl*	*negl*
v_n^{tot} fit ranges				0–1%	0–2%	0–1%

Table 1. Summary of systematic uncertainties for the v_2 of $\pi^{\pm}$, $K^{\pm}$, $p+\bar{p}$, $\Lambda+\overline{\Lambda}$, K^0_S, and the ϕ-meson. The uncertainties depend on p_{T} and centrality range; minimum and maximum values are listed here. Empty fields indicate that a given check does not apply to the particle of interest. If an uncertainty has been tested but cannot be resolved within statistical precision, the field is marked *negl* for negligible. Horizontal lines are used to separate the different categories of systematic uncertainties as explained in section 3.

more than one particle species simultaneously for $p_{\mathrm{T}} < 4\,\mathrm{GeV}/c$; (iii) varying the particle identification criterion from $n\sigma_{\mathrm{PID}} < 3$ to $n\sigma_{\mathrm{PID}} < 1$, $n\sigma_{\mathrm{PID}} < 2$, and $n\sigma_{\mathrm{PID}} < 4$; (iv) varying the $n\sigma_{\mathrm{TPC}}$ ranges that are used for particle identification for $p_{\mathrm{T}} > 4\,\mathrm{GeV}/c$.

The V^0 finding and ϕ-meson reconstruction. The nominal V^0 finding strategy is described in section 2.3. The V^0 finding criteria fall into two categories: topological requirements on the V^0s themselves, and selection imposed on their daughter tracks. These criteria are varied by (i) requiring a minimum p_{T} of the V^0 daughter tracks of $0.2\,\mathrm{GeV}/c$;

Error source	$\pi^\pm$	$K^\pm$	$p+\overline{p}$	K^0_S	$\Lambda+\overline{\Lambda}$
Vertex position	0–2%	0–1%	0–2%	0–3%	0–9%
1% wide centrality intervals	0–2%	0–2%	0–2%		
Centrality estimator	0–2%	0–2%	0–2%	0–4%	0–9%
Magnetic field polarity	0–2%	0–1%	0–3%	0–3%	0–3%
Interaction rate	1–2%	1–2%	1–3%	*negl*	*negl*
Pileup rejection	0–2%	0–1%	0–3%	0–1%	0–2%
Tracking mode	0–3%	1–5%	0–10%		
Number of TPC space points	0–1%	0–2%	0–5%	0–3%	0–6%
Track quality	1–3%	1–2%	1–3%	0–3%	0–6%
Particle identification purity	0–4%	1–3%	0–10%	0–4%	0–4%
Number of TPC clusters used for dE/dx	0–5%	0–5%	0–5%		
Exclusive particle identification	0–1%	0–2%	0–1%		
Decay vertex (radial position)				0–9%	0–11%
Armenteros-Podolanski variables				0–4%	
DCA decay products to primary vertex				0–3%	0–5%
DCA between decay products				0–5%	0–8%
Pointing angle $\cos\theta_p$				0–5%	0–1%
Minimum p_T of daughter tracks				0–4%	*negl*
Peak shape				*negl*	*negl*
Residual background in yield				*negl*	*negl*
Positive and negative rapidities	0–2%	0–1%	0–3%	0–5%	0–4%
Opposite charges	0–2%	0–2%	0–2%		
v_n from V0A or V0C	0–2%	0–1%	0–2%	0–4%	0–3%
Channel removal from V0A	0–8%	1–8%	1–8%	0–4%	0–5%
v_n^{bg} parametrization				*negl*	*negl*
v_n^{tot} fit ranges				0–2%	0–2%

Table 2. Summary of systematic uncertainties for the v_3 of $\pi^\pm$, $K^\pm$, $p+\overline{p}$, $\Lambda+\overline{\Lambda}$, and K^0_S. The uncertainties depend on p_T and centrality range; minimum and maximum values are listed here. Empty fields indicate that a given check does not apply to the particle of interest. If an uncertainty has been tested but cannot be resolved within statistical precision, the field is marked *negl* for negligible. Horizontal lines are used to separate the different categories of systematic uncertainties as explained in section 3.

(ii) changing the requirement on the minimum number of TPC space points that are used in the reconstruction of the V^0 daughter tracks form 70 to 60 and 80; (iii) varying the minimum number of TPC padrows crossed by the V^0 daughter tracks from 70 to 60 and 80; (iv) requesting at least 90% or 70% instead of 80% of the expected TPC space points to reconstruct the V^0 daughter tracks; (v) changing the maximum DCA of the V^0 daughter tracks to the secondary vertex from 0.5 cm to 0.3 cm and 0.7 cm; (vi) changing the minimum DCA of the V^0 daughter tracks to the primary vertex from 0.1 cm to 0.05 cm

Error source	$\pi^{\pm}$	$K^{\pm}$	$p+\overline{p}$
Vertex position	1–3%	1–3%	1–3%
1% wide centrality intervals	0–1%	0–1%	0–1%
Centrality estimator	1–3%	1–3%	2–3%
Magnetic field polarity	1–2%	1–3%	1–3%
Interaction rate	1–2%	2–3%	2–3%
Pileup rejection	0–2%	1–2%	2–3%
Tracking mode	0–2%	1–5%	1–10%
Number of TPC space points	0–1%	0–1%	0–1%
Track quality	3–4%	2–3%	3–4%
Particle identification purity	1–4%	2–4%	2–5%
Number of TPC clusters used for dE/dx	0–2%	0–1%	0–1%
Exclusive particle identification	0–1%	0–2%	0–1%
Positive and negative rapidities	1–3%	1–2%	2–3%
Opposite charges	2–3%	2–3%	2–3%
v_n from V0A or V0C	1–3%	2–4%	2–4%
Channel removal from V0A	6–14%	6–14%	5–15%

Table 3. Summary of systematic uncertainties for the v_4 of $\pi^{\pm}$, $K^{\pm}$, and $p+\overline{p}$. The uncertainties depend on p_T and centrality range; minimum and maximum values are listed here. Horizontal lines are used to separate the different categories of systematic uncertainties as explained in section 3.

and 0.3 cm; (vii) varying the number of clusters in the TPC that are used to estimate the dE/dx of the V^0 daughter tracks from 70 to 60 and 90; (viii) varying the particle identification criterion of the V^0 daughter tracks from $|n\sigma_{TPC}| < 3$ to $|n\sigma_{TPC}| < 1$ and $|n\sigma_{TPC}| < 4$; (ix) changing the minimum value of the $\cos\theta_p$ from 0.998 to 0.98; (x) varying the minimum radial distance to the primary vertex at which the V^0 can be produced from 5 cm to 1 cm and 15 cm; (xi) varying the maximum radial distance to the beam pipe at which the V^0 can be produced from 100 cm to 50 cm and 150 cm; (xii) the contamination from $\Lambda+\overline{\Lambda}$ decays and γ-conversions to the K_S^0 sample is checked by only selecting V^0 daughter tracks with a dE/dx value 2σ away from the expected electron dE/dx, effectively excluding electrons, and limiting the value of the Armenteros-Podolanski variables α and q.

The yield extraction, as explained in section 2.3 for the K_S^0 and $\Lambda+\overline{\Lambda}$, and section 2.4 for the ϕ-meson, is varied by: (i) using a third-order polynomial as parametrization of residual background in the invariant mass spectra; (ii) using for the ϕ-meson a Voigtian distribution (a convolution of a Gaussian distribution and Breit-Wigner distribution, where the width of the Breit-Wigner distribution is set to the natural width of the ϕ-meson, allowing for the Gaussian distribution to describe the smearing of the ϕ-meson width due to the detector resolution) for the parametrization of the ϕ-meson invariant mass yield; using for the K_S^0 and $\Lambda+\overline{\Lambda}$ a sum of two Gaussian distributions with the same mean for the parametrization of the K_S^0, $\Lambda+\overline{\Lambda}$ invariant mass yield; (iii, for the ϕ-meson only) using the yield of like-sign kaon pairs, in which two kaons with equal charge from the same event are used as candidate, for background yield description instead of event mixing.
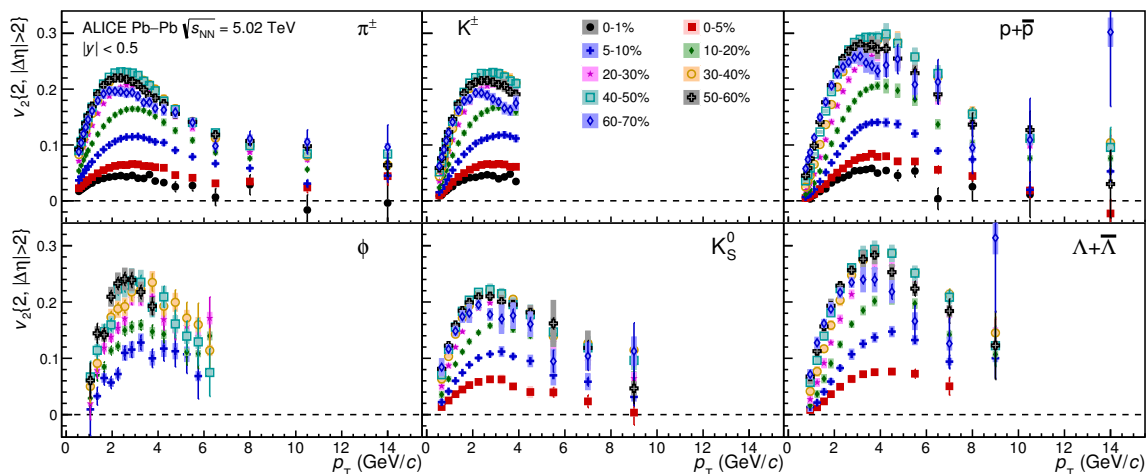
Figure 2. (Colour online) Centrality dependence of $v_2(p_T)$ for $\pi^\pm$, $K^\pm$, p+$\overline{p}$, Λ+$\overline{\Lambda}$, K_S^0, and the ϕ-meson. Statistical and systematic uncertainties are shown as bars and boxes, respectively.

Extraction of the $v_n(p_T)$. The nominal approach of measuring $v_n(p_T)$ is outlined in section 2.5, and is varied by: (i) performing flow analysis for $\pi^\pm$, $K^\pm$, and p+$\overline{p}$ for positive and negative charges independently; (ii) performing flow analysis for positive and negative rapidities independently; (iii) performing flow analysis for $\pi^\pm$, $K^\pm$, and p+$\overline{p}$ in 1% centrality intervals and merging the result rather than measuring in wider centrality intervals directly; (iv) suppressing the signal from a specific V0A channel in the evaluation of the $\mathbf{Q}_n$-vector (see eq. (2.2)), which, on average, measures a lower energy deposition with respect to the ones reported by the other channels from the same ring; (v) performing flow analysis with the $\mathbf{Q}_n$-vector calculated from the V0A or V0C separately; (vi) testing various $M_{d^+d^-}$ intervals over which $v_n^{\text{bg}}(M_{d^+d^-})$ is fitted; (vii) testing the assumption made on v_n^{bg} by changing the parametrization from a second-order polynomial to a first-order polynomial function.

4 Results and discussion

The flow coefficients v_2, v_3, and v_4 of identified particles are presented for various centrality classes in section 4.1; scaling properties are discussed in section 4.2. Comparisons to various model calculations, studies on the shape evolution of $v_n(p_T)$ with centrality, and comparisons to v_n measured at $\sqrt{s_{NN}} = 2.76$ TeV are shown in sections 4.3, 4.4, and 4.5, respectively.

4.1 Centrality and p_T dependence of flow coefficients

Figure 2 shows the $v_2(p_T)$ of $\pi^\pm$, $K^\pm$, p+$\overline{p}$, Λ+$\overline{\Lambda}$, K_S^0, and the ϕ-meson for various centrality classes in the range 0–70%. For the $\pi^\pm$, $K^\pm$ and p+$\overline{p}$, measurements performed in ultra-central collisions (0–1%) are also presented. For the ϕ-meson, the results are reported in the 5–60% centrality range, where v_2 can be measured accurately. The magnitude of v_2 increases strongly with decreasing centrality up to the 40–50% centrality interval for all particle species. This evolution is expected, since the eccentricity of the overlap zone of the
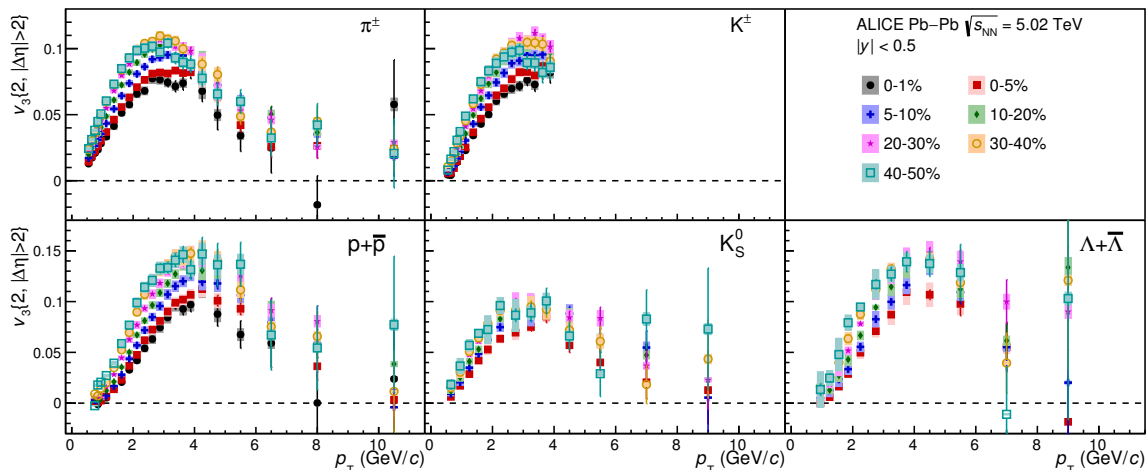
Figure 3. (Colour online) Centrality dependence of $v_3(p_T)$ for $\pi^\pm$, $K^\pm$, p+$\overline{p}$, $\Lambda+\overline{\Lambda}$, and K^0_S. Statistical and systematic uncertainties are shown as bars and boxes, respectively.
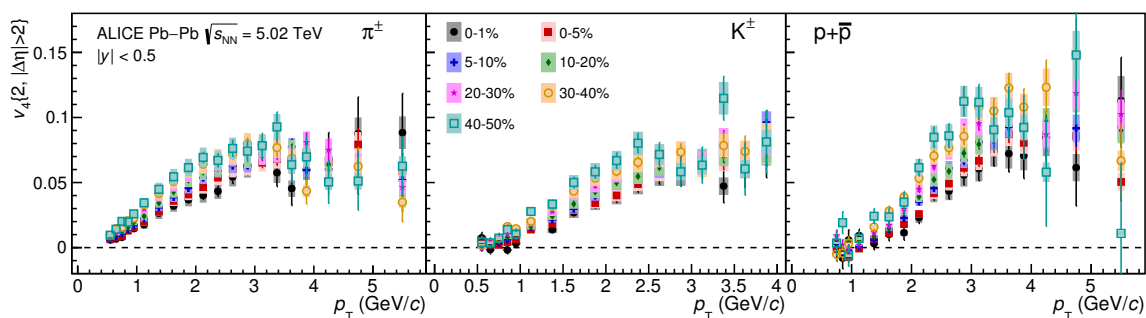

Figure 4. (Colour online) Centrality dependence of $v_4(p_T)$ for $\pi^\pm$, $K^\pm$, and p+$\overline{p}$. Statistical and systematic uncertainties are shown as bars and boxes, respectively.

colliding nuclei increases for peripheral collisions and v_2 scales approximately linearly with eccentricity [77]. For more peripheral collisions (i.e. 50–60% and 60–70%), the value of v_2 is smaller than in the previous centrality intervals for all particle species except the ϕ-meson. This suggests that the system has a shorter lifetime in more peripheral collisions, which does not allow for the generation of large v_2 [78]. Furthermore, the reduced contribution of eccentricity fluctuations and hadronic interactions might play an important role in these centrality ranges [79]. A non-zero, positive v_2 is found in the 0–1% centrality interval for $p_T < 6$ GeV/c for $\pi^\pm$, $K^\pm$, and p+$\overline{p}$, which mostly reflects the contribution from event-by-event fluctuations in the initial nucleon and gluon density as the system shape is almost spherical at vanishing impact parameter.

The third-order flow coefficent v_3 is generated by inhomogeneities in the initial nucleon and gluon density and not by the collision geometry [12–15], while v_4 arises from initial collision geometry, fluctuations, and the non-linear hydrodynamic response of the medium [16, 17]. Higher-order flow harmonics are more sensitive to transport coefficients than v_2 [15], as the dampening effect of η/s leads to a stronger decrease of these coefficients [18, 19]. Figures 3 and 4 present the $v_3(p_T)$ of $\pi^\pm$, $K^\pm$, p+$\overline{p}$, $\Lambda+\overline{\Lambda}$, and K^0_S and

$v_4(p_{\rm T})$ of $\pi^\pm$, $\mathrm{K}^\pm$, and $\mathrm{p}+\overline{\mathrm{p}}$ for various centrality classes in the 0–50% range. Statistical precision limits extending the v_4 measurement to more peripheral collisions or carrying it out for $\Lambda+\overline{\Lambda}$, $\mathrm{K}^0_{\rm S}$, and the ϕ-meson. Non-zero, positive v_3 and v_4 are observed for particle species throughout the entire $p_{\rm T}$ ranges up to ≈ 8 GeV/c. Unlike v_2, the coefficients v_3 and v_4 increase weakly from ultra-central to peripheral collisions. This observation illustrates that higher-order flow coefficients are mainly generated by event-by-event fluctuations in the initial nucleon and gluon density.

All flow coefficients increase monotonically with increasing $p_{\rm T}$ up to 3–4 GeV/c where a maximum is reached. The position of this maximum depends on centrality and particle species as it takes place at higher $p_{\rm T}$ for heavier particles for various centrality classes. This behaviour can be explained by the centrality dependence of radial flow combined with the parton density, which will be detailed in section 4.4.

Figure 5 presents the evolution of $v_{\rm n}(p_{\rm T})$ of different particle species for various centrality classes. In the most central collisions, initial nucleon-density fluctuations are expected to be the main contributor to the generation of $v_{\rm n}$. For the 0–1% centrality interval, v_3 is the dominant flow coefficient for $1.5 < p_{\rm T} < 6.0$ GeV/c, $2.0 < p_{\rm T} < 4$ GeV/c, and $2.5 < p_{\rm T} < 6$ GeV/c for $\pi^\pm$, $\mathrm{K}^\pm$, and $\mathrm{p}+\overline{\mathrm{p}}$, respectively. Furthermore, v_4 becomes equal to v_2 at $p_{\rm T} \approx 2.0$ GeV/c (2.2, 2.5) for $\pi^\pm$ ($\mathrm{K}^\pm$, $\mathrm{p}+\overline{\mathrm{p}}$), after which it increases gradually and reaches a magnitude similar to v_3 at around 3.5 GeV/c. A similar trend is observed in the 0–5% centrality class for all particle species. However, the crossing between flow coefficients (the $p_{\rm T}$ value at which they reach a similar magnitude), which also depends on the particle mass, takes place at different $p_{\rm T}$ values than for the 0–1% centrality interval. This dependence of the crossing between different flow coefficients can be attributed to the interplay of elliptic, triangular, and quadrangular flow with radial flow. Upwards of 5% collision centrality, v_2 is larger than v_3 and v_4, confirming the hypothesis that collision geometry dominates the generation of flow coefficients.

Figure 6 shows the $v_2(p_{\rm T})$ of $\pi^\pm$, $\mathrm{K}^\pm$, $\mathrm{p}+\overline{\mathrm{p}}$, $\Lambda+\overline{\Lambda}$, $\mathrm{K}^0_{\rm S}$, and the ϕ-meson in a given centrality interval arranged into panels of various centrality classes, which allows for further illustration of the interplay between elliptic and radial flow. For $p_{\rm T} < 2$–3 GeV/c, v_2 of the different particle species is mass-ordered, meaning that lighter particles have a larger v_2 than heavier particles at the same $p_{\rm T}$. This behaviour is indicative of strong radial flow which imposes an equal, isotropic velocity boost to all particles in addition to the anisotropic expansion of the medium [20–22]. For $3 < p_{\rm T} < 8$–10 GeV/c, particles are grouped according to their number of constituent quarks, which supports the hypothesis of particle production via quark coalescence [34]. Particle type scaling and mass ordering are most directly tested by the ϕ-meson v_2, as its mass is close to the proton mass. Figure 6 demonstrates that the ϕ-meson v_2 follows proton v_2 at low $p_{\rm T}$, but pion v_2 at intermediate $p_{\rm T}$ in all centrality classes. The crossing between meson and baryon v_2, which depends on the particle species, happens at higher $p_{\rm T}$ values for central than peripheral collisions as a result of the larger radial flow in the former. Lastly, it is seen that the v_2 of baryons is higher than that of mesons up to $p_{\rm T} \approx 10$ GeV/c, indicating that particle type dependence of v_2 persists up to high $p_{\rm T}$. For $p_{\rm T} > 10$ GeV/c, where v_2 depends only weakly on transverse momentum, the magnitude of $\mathrm{p}+\overline{\mathrm{p}}$ v_2 is compatible with that for
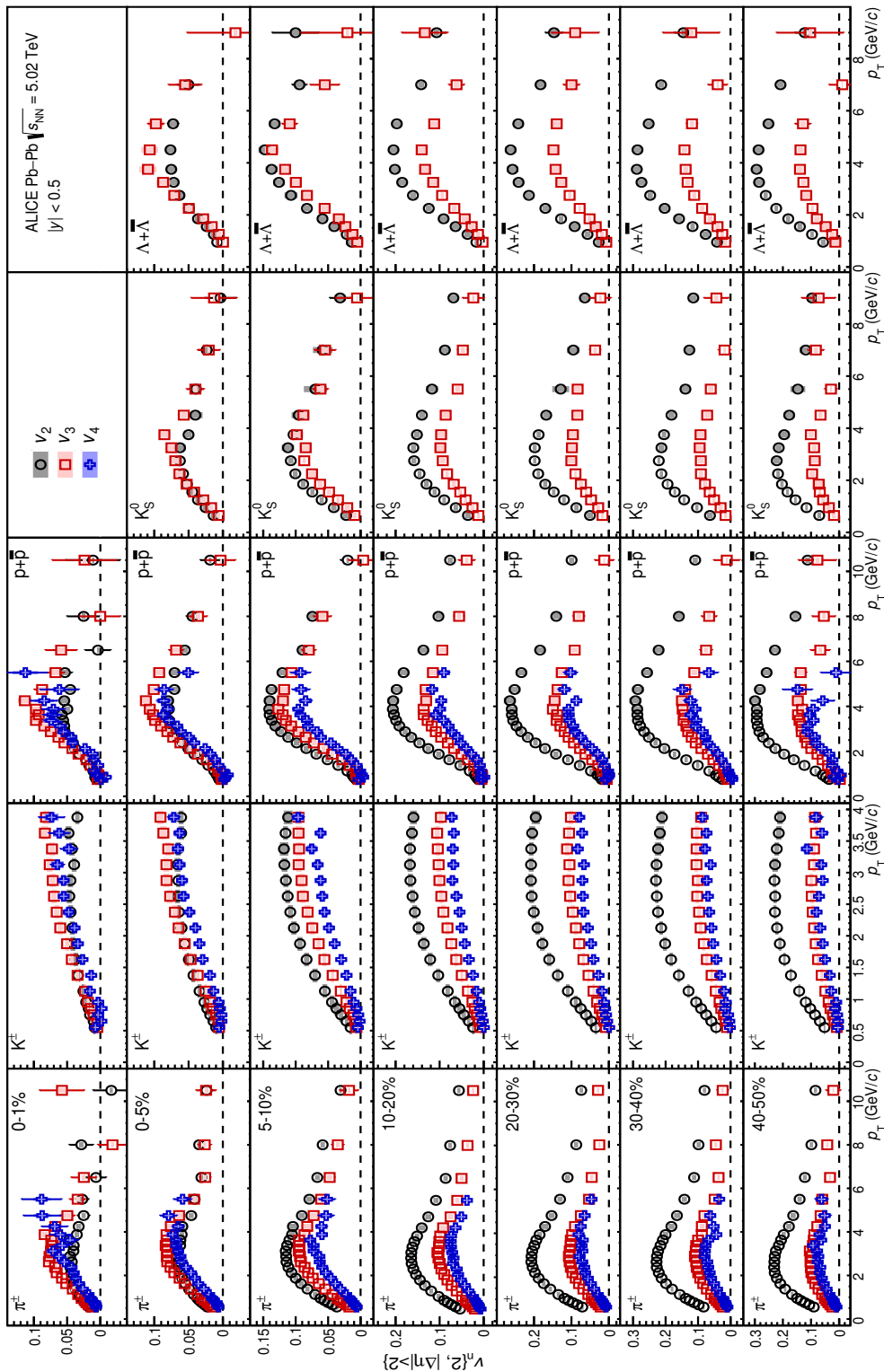
Figure 5. (Colour online) The evolution of $v_n(p_T)$ of $\pi^\pm$, $K^\pm$, $p+\bar{p}$, $\Lambda+\bar{\Lambda}$, and K_S^0 for various centrality classes. Statistical and systematic uncertainties are shown as bars and boxes, respectively.
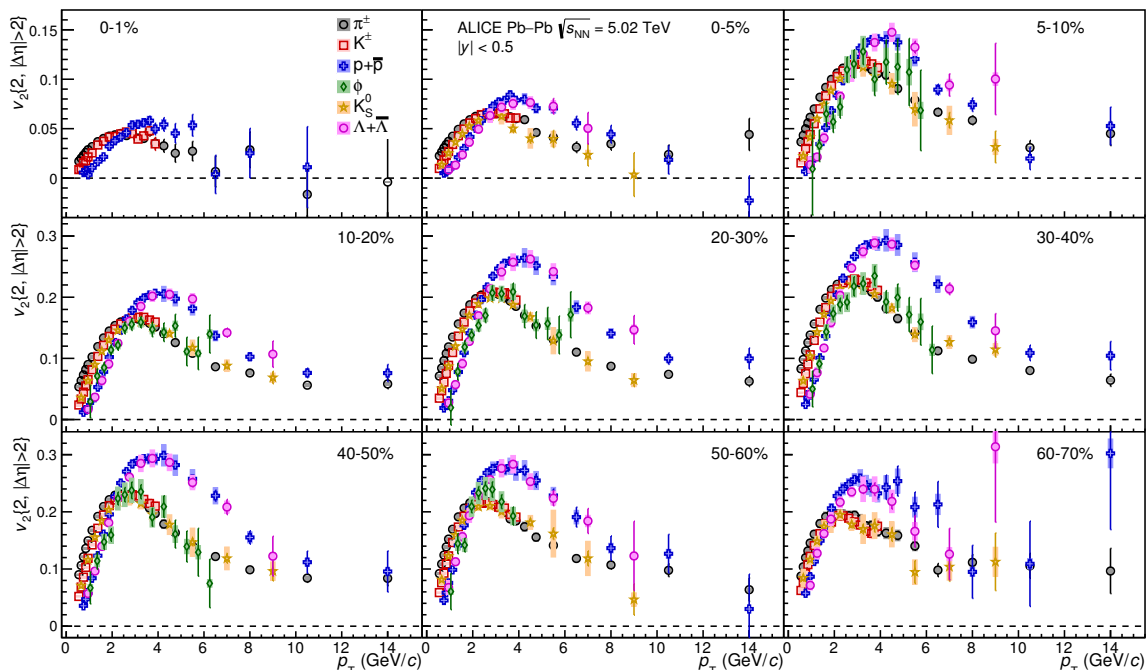
Figure 6. (Colour online) The p_{T}-differential v_2 of $\pi^{\pm}$, $\mathrm{K}^{\pm}$, $\mathrm{p}+\overline{\mathrm{p}}$, $\Lambda+\overline{\Lambda}$, $\mathrm{K}_{\mathrm{S}}^0$, and the ϕ-meson for various centrality classes. Statistical and systematic uncertainties are shown as bars and boxes, respectively.

$\pi^{\pm}$ within statistical and systematic uncertainties. Furthermore, the nuclear modification factor in this high p_{T} region is found to be the same for the two particle species within uncertainties [80].

Figures 7 and 8 present the $v_3(p_{\mathrm{T}})$ and $v_4(p_{\mathrm{T}})$ for different particle species in a given centrality interval. Both v_3 and v_4 show a clear mass ordering at $p_{\mathrm{T}} < 2$–$3\,\mathrm{GeV}/c$, confirming the interplay between triangular and quadrangular flow and radial flow. For $3 < p_{\mathrm{T}} < 8\,\mathrm{GeV}/c$, particles are grouped into mesons and baryons and, analogous to the trend of v_2 in this p_{T} region, the flow of baryons is larger than that of mesons. The crossing between meson and baryon v_3 and v_4 also exhibits a centrality and particle mass dependence.

Figures 6 and 7 also show a comparison between $\mathrm{K}^{\pm}$ and $\mathrm{K}_{\mathrm{S}}^0$ v_2 and v_3 as a function of p_{T} for various centrality classes. A difference in $v_n(p_{\mathrm{T}})$ is found between the $\mathrm{K}^{\pm}$ and $\mathrm{K}_{\mathrm{S}}^0$ measurements: the magnitude of $\mathrm{K}_{\mathrm{S}}^0$ v_n is systematically smaller than the magnitude of $\mathrm{K}^{\pm}$ v_n. This difference in v_n exhibits no p_{T} dependence, but changes with centrality for v_2. For $0.8 < p_{\mathrm{T}} < 4.0$ GeV/c, the difference in v_2 ranges from $7\% \pm 3.5\%(\mathrm{syst}) \pm 0.7\%(\mathrm{stat})$ in the most central collisions to $1.5\% \pm 1.5\%(\mathrm{syst}) \pm 0.4\%(\mathrm{stat})$ in peripheral collisions. In the same kinematic range, a deviation in v_3 of $6.5\% \pm 5\%(\mathrm{syst}) \pm 1.7\%(\mathrm{stat})$ is found in the most central collisions and of $6\% \pm 4.5\%(\mathrm{syst}) \pm 1\%(\mathrm{stat})$ in peripheral collisions. This difference is similar in magnitude and centrality dependence as the one reported by ALICE in Pb-Pb collisions at $\sqrt{s_{\mathrm{NN}}} = 2.76\,\mathrm{TeV}$ in [27].
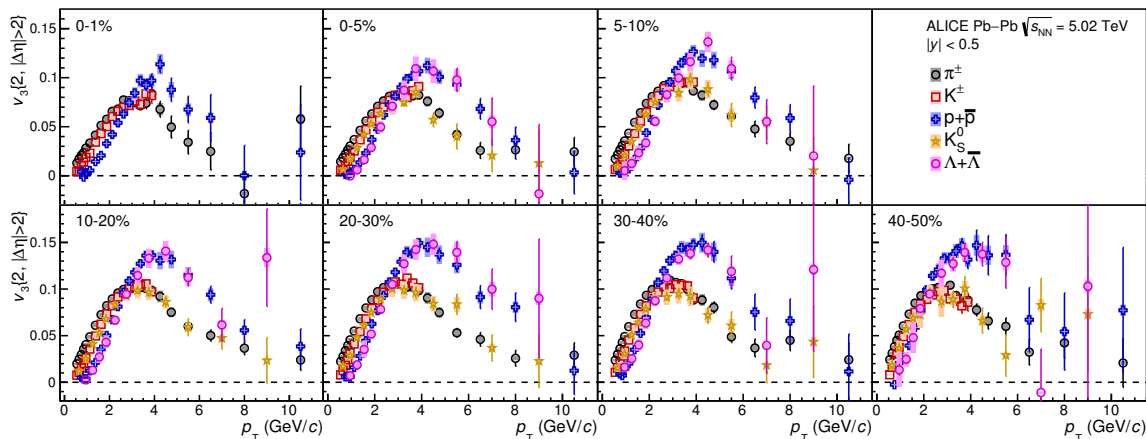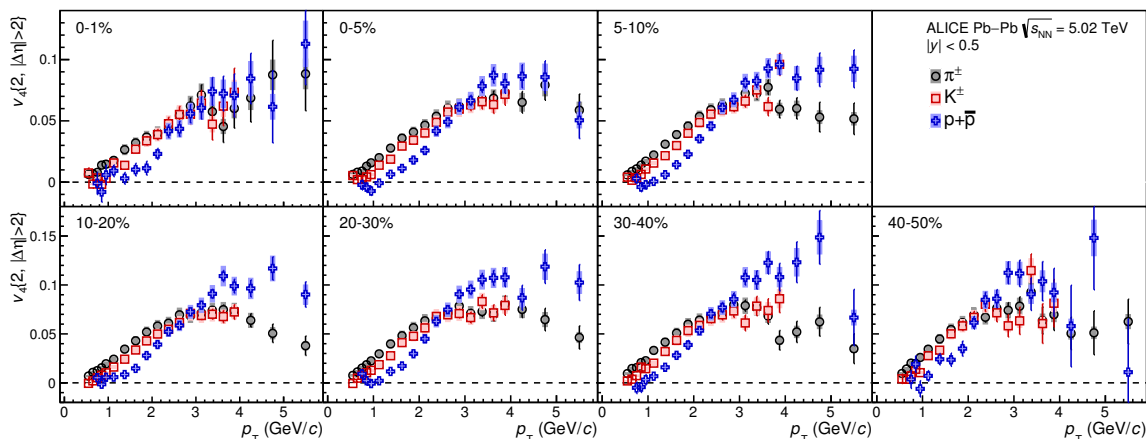
Figure 7. (Colour online) The p_T-differential v_3 of $\pi^\pm$, $K^\pm$, p+$\overline{p}$, $\Lambda+\overline{\Lambda}$, and K^0_S for various centrality classes. Statistical and systematic uncertainties are shown as bars and boxes, respectively.

Figure 8. (Colour online) The p_T-differential v_4 of $\pi^\pm$, $K^\pm$, and p+$\overline{p}$ for various centrality classes. Statistical and systematic uncertainties are shown as bars and boxes, respectively.

4.2 Scaling properties

To test the hypothesis of particle production via quark coalescence [34], which would lead to a grouping of v_n of mesons and baryons at intermediate p_T, both v_n and p_T are divided by the number of constituent quarks (n_q) independently for each particle species. The v_2/n_q, v_3/n_q, and v_4/n_q of $\pi^\pm$, $K^\pm$, p+$\overline{p}$, $\Lambda+\overline{\Lambda}$, K^0_S, and the ϕ-meson, plotted as a function of p_T/n_q, are reported in figures 9, 10, and 11 for various centrality classes.

For $p_T/n_q > 1$ GeV/c, the scaling is only approximate. To quantify the degree to which the measurements deviate from the n_q scaling, the p_T/n_q dependence of v_n/n_q has been divided by a cubic spline fit to the p+$\overline{p}$ v_n/n_q. In the region where quark coalescence is hypothesized to be the dominant process ($\approx 1 < p_T/n_q < 3$ GeV/c) [34, 81], a deviation from the exact scaling of $\pm$ 20% is found for v_2 for central collisions, which decreases to $\pm$15% for the most peripheral collisions. For higher harmonics, a $\pm$20% deviation is found for all centrality classes. This deviation is in agreement with earlier observations [27, 28, 32].
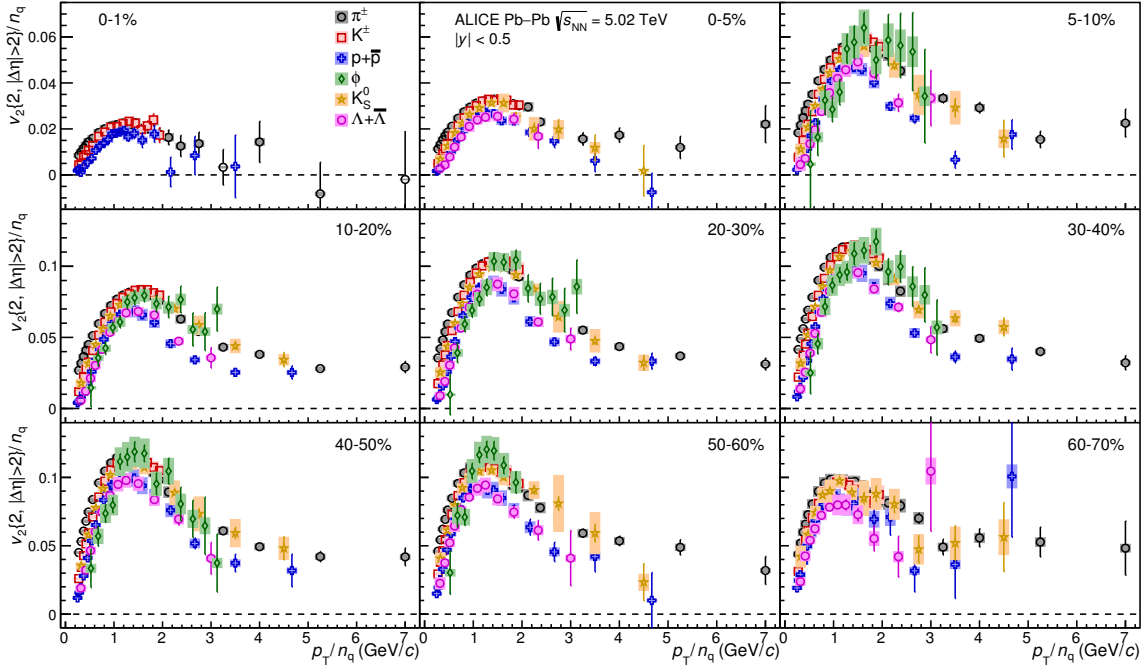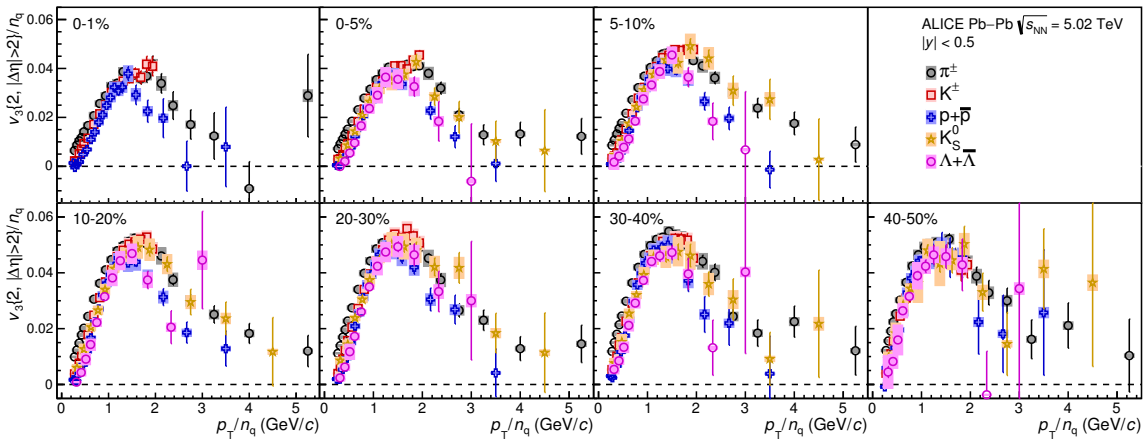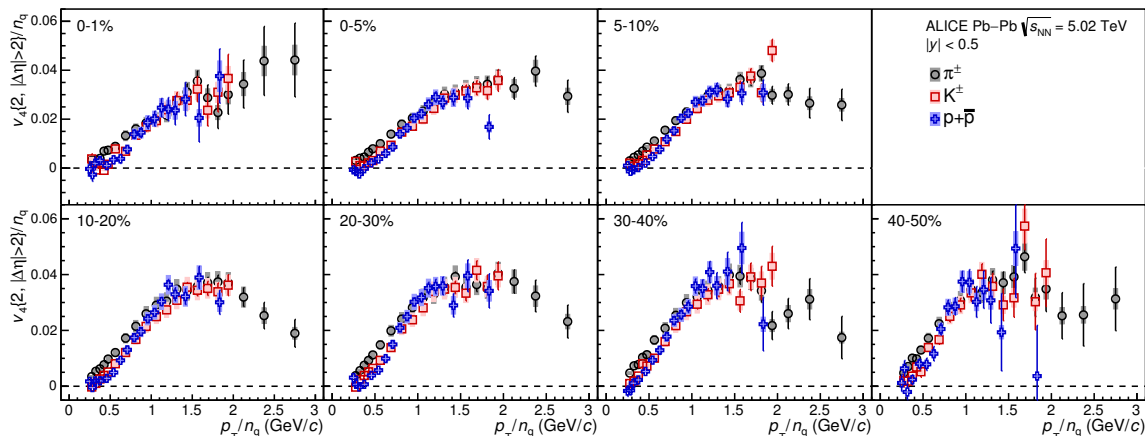
Figure 9. (Colour online) The p_T/n_q dependence of v_2/n_q of $\pi^\pm$, $K^\pm$, $p+\overline{p}$, $\Lambda+\overline{\Lambda}$, K^0_S, and the ϕ-meson for various centrality classes. Statistical and systematic uncertainties are shown as bars and boxes, respectively.

Figure 10. (Colour online) The p_T/n_q dependence of v_3/n_q of $\pi^\pm$, $K^\pm$, $p+\overline{p}$, $\Lambda+\overline{\Lambda}$, and K^0_S for various centrality classes. Statistical and systematic uncertainties are shown as bars and boxes, respectively.

Figure 11. (Colour online) The p_T/n_q dependence of v_4/n_q of $\pi^\pm$, $K^\pm$, and p+$\overline{p}$ for various centrality classes. Statistical and systematic uncertainties are shown as bars and boxes, respectively.

4.3 Comparison with model calculations

To test the validity of the hydrodynamic description of the QGP evolution, the v_n measurements in the 0–5%, 10–20% and 40–50% centrality intervals are compared to hydrodynamical calculations in figures 12, 13, and 14 for $\pi^\pm$, $K^\pm$, and p+$\overline{p}$, respectively. Predictions from MUSIC [82] and iEBE-VISHNU [83] simulations are depicted by the different coloured curves. The first calculation is based on MUSIC [84], an event-by-event 3+1 dimensional viscous hydrodynamic model, coupled to a hadronic cascade model (UrQMD) [85, 86], which allows the influence of the hadronic phase on the anisotropic flow to be studied for different particle species. The IP-Glasma model [87, 88] is used to simulate the initial conditions of the collision. MUSIC uses a starting time for the hydrodynamic evolution of $\tau_0 = 0.4\,\text{fm}/c$, a switching temperature between the macroscopic hydrodynamic description and the microscopic transport evolution of $T_{\text{sw}} = 145\,\text{MeV}$, a value of $\eta/s = 0.095$, and a temperature dependent ζ/s. The second calculation employs the iEBE-VISHNU hybrid model [89], which is an event-by-event version of the VISHNU hybrid model [90], and couples 2+1 dimensional viscous hydrodynamics VISH2+1 [78] to UrQMD. The T$_\text{R}$ENTo [91] and AMPT [92] models are used to describe the initial conditions. For both configurations, $\tau_0 = 0.6\,\text{fm}/c$ and $T_{\text{sw}} = 148\,\text{MeV}$ are set from [93], where these values have been obtained utilizing Bayesian statistics from a simultaneous fit of final charged-particle density, mean transverse momentum, and integrated flow coefficients v_n in Pb-Pb collisions at $\sqrt{s_{\text{NN}}} = 2.76\,\text{TeV}$. The temperature-dependent η/s and ζ/s extracted in [93] are used for T$_\text{R}$ENTo initial conditions, while $\eta/s = 0.08$ and $\zeta/s = 0$ are taken for AMPT.

Figures 12, 13, and 14 show that the hydrodynamical calculations qualitatively reproduce the v_n measurements. The differences between the data points and models are visualized in figures 12, 13, and 14 as the ratios of the measured v_n to a fit to the theoretical calculations. The iEBE-VISHNU calculations using AMPT initial conditions describe the p_T-differential v_n of $\pi^\pm$, $K^\pm$, and p+$\overline{p}$ more accurately than T$_\text{R}$ENTo based and MUSIC calculations for $p_T > 1\,\text{GeV}/c$. Using AMPT initial conditions, there is good agreement
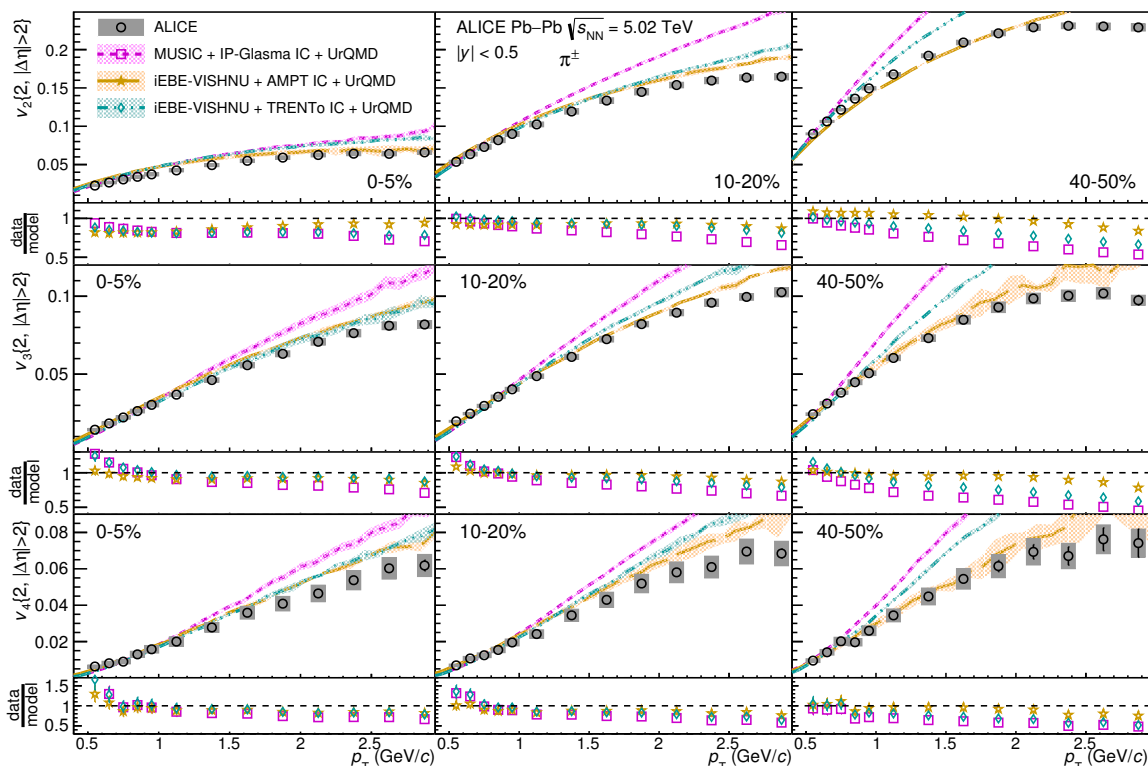
Figure 12. (Colour online) The p_{T}-differential v_2 (top), v_3 (middle), and v_4 (bottom) of $\pi^{\pm}$ for the 0–5%, 10–20%, and 40–50% centrality classes compared to hydrodynamical calculations from MUSIC model using IP-Glasma initial conditions (magenta) [82] and the iEBE-VISHNU hybrid model using AMPT (orange) or T$_{\mathrm{R}}$ENTo (cyan) initial conditions [83]. Statistical and systematic uncertainties of the data points are shown as bars and boxes, respectively. The uncertainties of the hydrodynamical calculations are depicted by the thickness of the curves. The ratios of the measured v_{n} to a fit to the hydrodynamical calculations are also presented for clarity.

between $\pi^{\pm}$ and $\mathrm{K}^{\pm}$ v_{n} and iEBE-VISHNU calculations for $p_{\mathrm{T}} < 2\,\mathrm{GeV}/c$, while $\mathrm{p}+\overline{\mathrm{p}}$ v_{n} is described fairly well up to $p_{\mathrm{T}} = 3\,\mathrm{GeV}/c$. The T$_{\mathrm{R}}$ENTo based predictions follow $\pi^{\pm}$ and $\mathrm{K}^{\pm}$ v_{n} up to slightly lower transverse momenta ($p_{\mathrm{T}} < 1$–$2\,\mathrm{GeV}/c$) and to $p_{\mathrm{T}} < 3\,\mathrm{GeV}/c$ for $\mathrm{p}+\overline{\mathrm{p}}$, depending on the considered centrality interval. The MUSIC calculations are in agreement with the measured v_{n} for $p_{\mathrm{T}} < 1\,\mathrm{GeV}/c$ in central collisions, however they overestimate v_2 at lower p_{T} in more peripheral collisions.

4.4 Shape evolution of $v_{\mathrm{n}}(p_{\mathrm{T}})$ as function of centrality

The evolution of the shape of $v_{\mathrm{n}}(p_{\mathrm{T}})$ as function of centrality is quantified by taking the ratio of $v_{\mathrm{n}}(p_{\mathrm{T}})$ in a given centrality interval to the $v_{\mathrm{n}}(p_{\mathrm{T}})$ measured in the 20–30% centrality interval

$$v_{\mathrm{n}}(p_{\mathrm{T}})_{\text{ratio to }20-30\%} = \frac{v_{\mathrm{n}}(p_{\mathrm{T}})}{v_{\mathrm{n}}(p_{\mathrm{T}})|_{20-30\%}} \frac{v_{\mathrm{n}}|_{20-30\%}}{v_{\mathrm{n}}}, \tag{4.1}$$

where the second fraction on the right-hand side of the equation serves as a normalization factor which is constructed from the p_{T}-integrated v_{n} values obtained in the 20–30% centrality interval ($v_{\mathrm{n}}|_{20-30\%}$) and the centrality interval of interest (v_{n}). Centrality-dependent
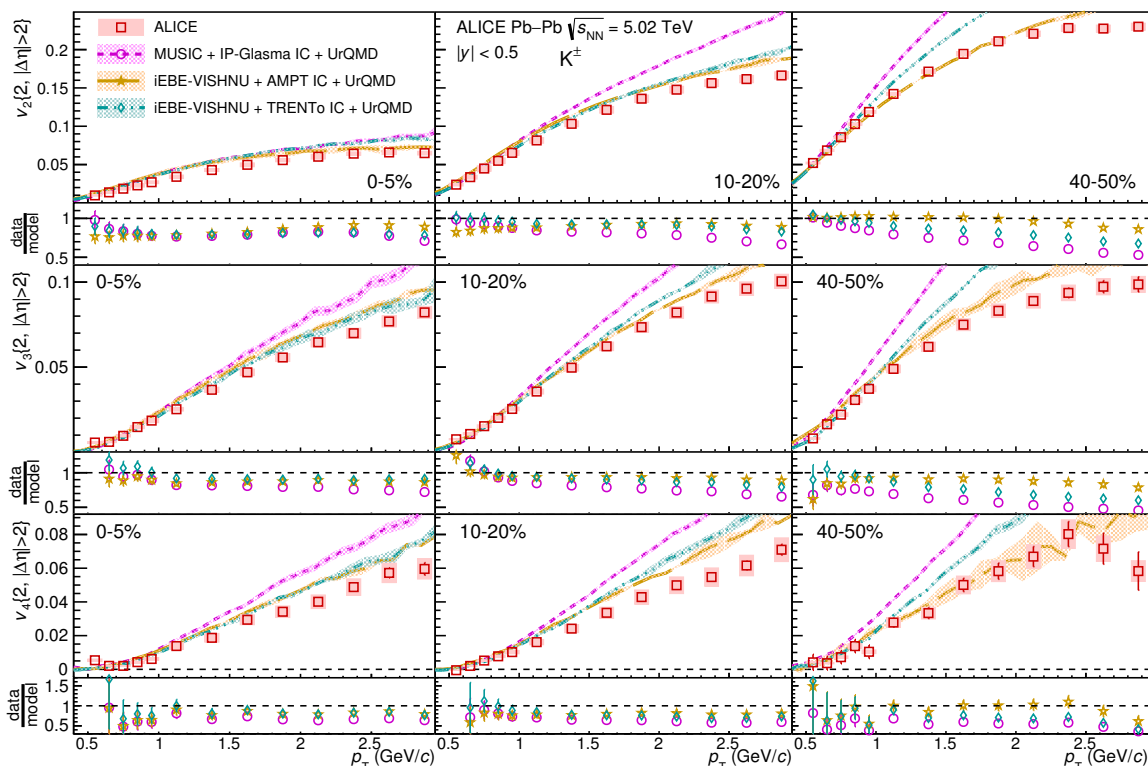
Figure 13. (Colour online) The p_T-differential v_2 (top), v_3 (middle), and v_4 (bottom) of $K^\pm$ for the 0–5%, 10–20%, and 40–50% centrality classes compared to hydrodynamical calculations from MUSIC model using IP-Glasma initial conditions (magenta) [82] and the iEBE-VISHNU hybrid model using AMPT (orange) or T$_R$ENTo (cyan) initial conditions [83]. Statistical and systematic uncertainties of the data points are shown as bars and boxes, respectively. The uncertainties of the hydrodynamical calculations are depicted by the thickness of the curves. The ratios of the measured v_n to a fit to the hydrodynamical calculations are also presented for clarity.

variations in the shape of $v_n(p_T)$ will present themselves as deviations from unity of the observed $v_n(p_T)_{\text{ratio to } 20-30\%}$.

The shape evolution of elliptic and triangular flow is shown in figures 15 and 16 for $\pi^\pm$, $K^\pm$, p+$\overline{\text{p}}$, and inclusive charged particles (the latter taken from [44]). For inclusive charged particles, variations in shape of about 10% are observed for $p_T < 3$ GeV/c, which increase to about 30% for $p_T < 6$ GeV/c. The shape evolution of $v_2(p_T)$ shows different trends for $\pi^\pm$, $K^\pm$, and p+$\overline{\text{p}}$. While $\pi^\pm$ $v_2(p_T)_{\text{ratio to } 20-30\%}$ follows inclusive charged particle over the considered p_T range, the elliptic flow of p+$\overline{\text{p}}$ ($K^\pm$) varies between 20% (10%) to 250% (55%) at low p_T from most central to peripheral collisions. The variations are more pronounced for $v_3(p_T)$, in particular for central collisions. The mass dependence found in the shape evolution of both v_2 and v_3 for $p_T < 4$ GeV/c can be attributed to variations of the magnitude of radial flow and quark density, both being larger for central than peripheral collisions. Radial flow has a stronger effect on the v_n of heavier particles than that of lighter particles at low p_T, while the quark density influences the peak value of $v_n(p_T)$ in the coalescence model picture [35, 36, 94]. For $p_T > 4$ GeV/c, the shape evolution shows little (if any) particle type dependence.
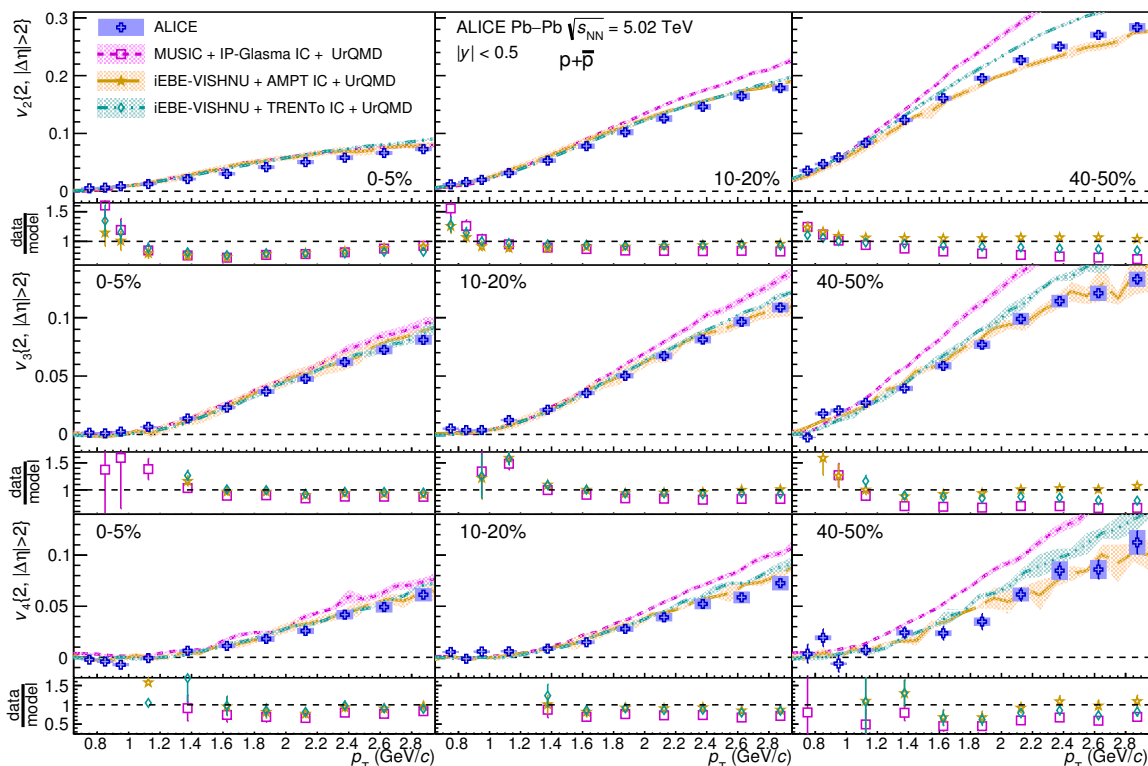
Figure 14. (Colour online) The p_T-differential v_2 (top), v_3 (middle), and v_4 (bottom) of p+$\overline{\text{p}}$ for the 0–5%, 10–20%, and 40–50% centrality classes compared to hydrodynamical calculations from MUSIC model using IP-Glasma initial conditions (magenta) [82] and the iEBE-VISHNU hybrid model using AMPT (orange) or T$_{\text{R}}$ENTo (cyan) initial conditions [83]. Statistical and systematic uncertainties of the data points are shown as bars and boxes, respectively. The uncertainties of the hydrodynamical calculations are depicted by the thickness of the curves. The ratios of the measured v_{n} to a fit to the hydrodynamical calculations are also presented for clarity.

The shape evolution of $v_2(p_T)$ for $\pi^{\pm}$, K$^{\pm}$, and p+$\overline{\text{p}}$ is compared to calculations from the MUSIC and iEBE-VISHNU hybrid models in figure 17. Both models describe the shape evolution for p+$\overline{\text{p}}$ over the p_T range $0.7 < p_T < 3$ GeV/c. The iEBE-VISHNU model reproduces the shape evolution for $\pi^{\pm}$ and K$^{\pm}$ for $p_T < 1.5$ GeV/c. Calculations from the MUSIC model deviate strongly from the observed shape evolution for $\pi^{\pm}$ and K$^{\pm}$ in peripheral collisions.

As quark density depends on centrality, the maximum v_{n} is expected to be found at higher p_T in more central collisions. To further quantify this aspect of the shape evolution of $v_{\text{n}}(p_T)$, the p_T of $\pi^{\pm}$, p+$\overline{\text{p}}$, $\Lambda + \overline{\Lambda}$, and K$_S^0$ where $v_2(p_T)$ and $v_3(p_T)$ reach a maximum, divided by number of constituent quarks n_{q}, is reported in figure 18 as a function of centrality. The ϕ-meson and K$^{\pm}$ are not included since the kinematic range and granularity of the measurements do not allow for a reliable extraction of a maximum. The left panel of figure 18 shows that the p_T/n_{q} at which $v_2(p_T)$ reaches a maximum, denoted as $p_T|_{v_2^{\max}}/n_{\text{q}}$, decreases with increasing centrality percentile for collision centralities larger than 5–10%, following the expectations from the hypothesis of hadronization
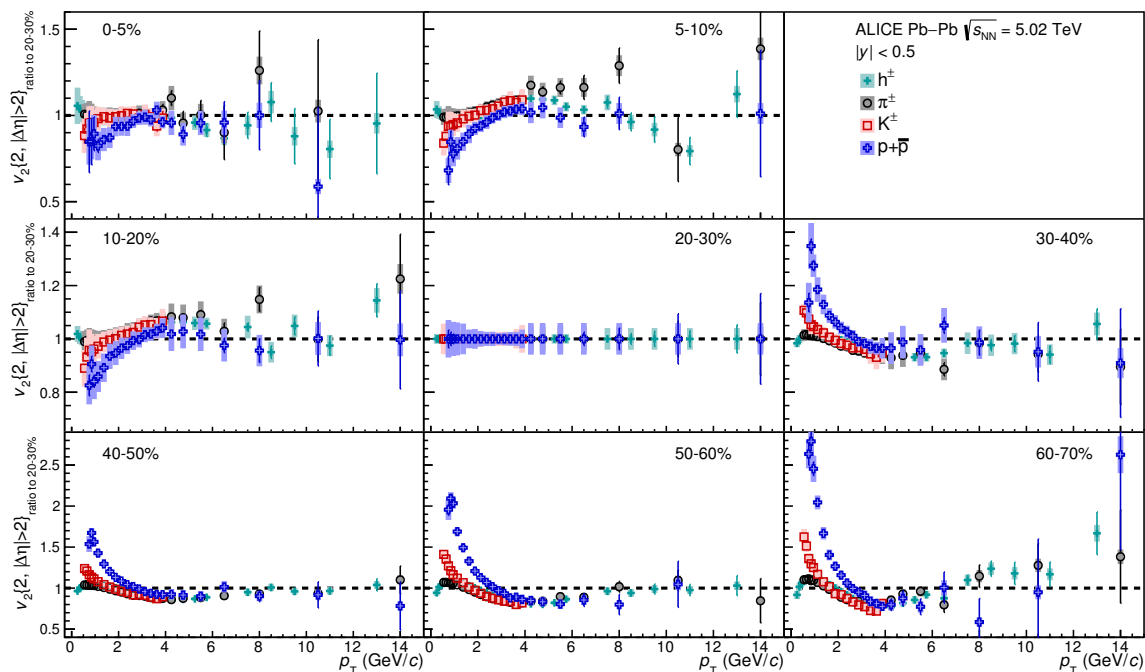
Figure 15. (Colour online) Centrality dependence of $v_2(p_{\mathrm{T}})_{\mathrm{ratio\ to\ 20-30\%}}$ for $\pi^{\pm}$, $\mathrm{K}^{\pm}$, $\mathrm{p}+\overline{\mathrm{p}}$, and inclusive charged particles [44]. Statistical and systematic uncertainties are shown as bars and boxes, respectively.

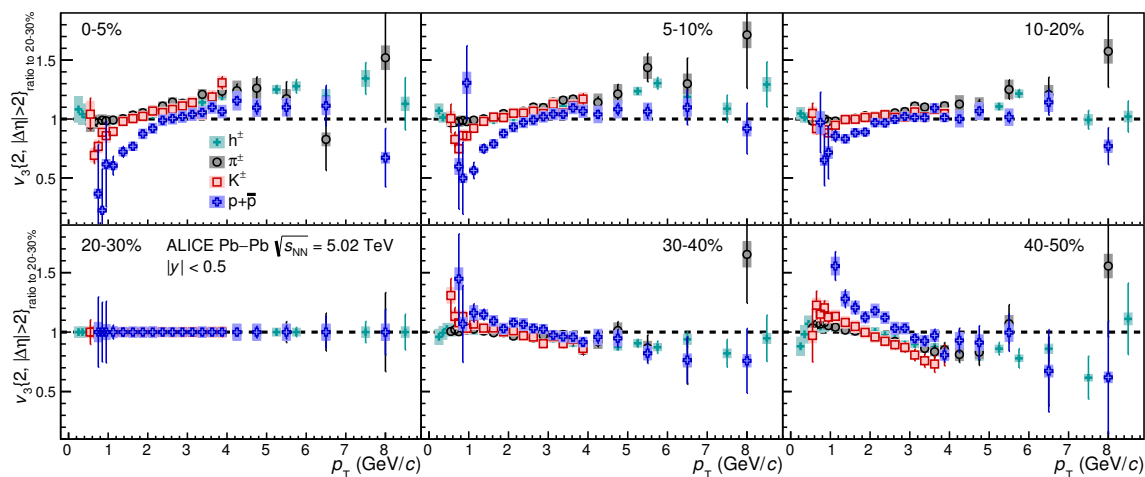**Figure 16**. (Colour online) Centrality dependence of $v_3(p_{\mathrm{T}})_{\mathrm{ratio\ to\ 20-30\%}}$ for $\pi^{\pm}$, $\mathrm{K}^{\pm}$, $\mathrm{p}+\overline{\mathrm{p}}$, and inclusive charged particles [44]. Statistical and systematic uncertainties are shown as bars and boxes, respectively.

through coalescence. The systematic uncertainties as presented in figure 18 have been evaluated directly on $p_{\mathrm{T}}|_{v_{\mathrm{n}}^{\max}}/n_{\mathrm{q}}$ to accurately take into account that some systematic uncertainties can be point-by-point correlated in p_{T}. In the 0–5% centrality interval, there is a hint of a lower $p_{\mathrm{T}}|_{v_2^{\max}}/n_{\mathrm{q}}$ than in the 5–10% centrality class for all particle species. The observed $p_{\mathrm{T}}|_{v_2^{\max}}/n_{\mathrm{q}}$ is compatible among all particle species with the exception of the
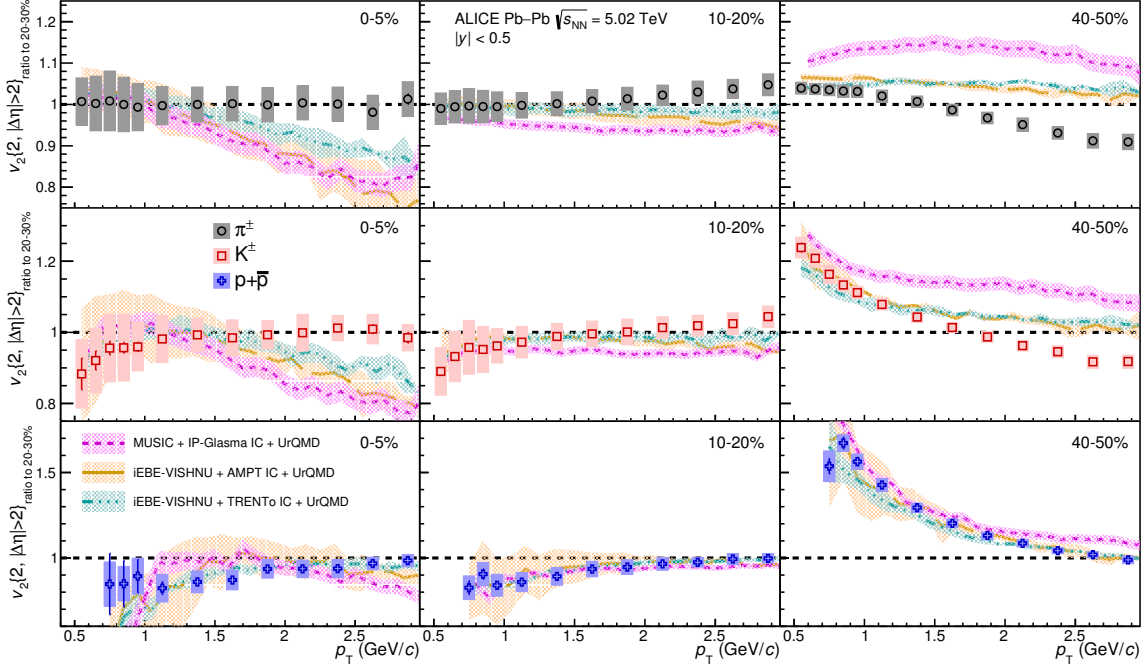
Figure 17. (Colour online) Centrality dependence of $v_2(p_T)_{\text{ratio to } 20-30\%}$ for $\pi^\pm$ (upper panels), $K^\pm$ (middle panels), and $p+\bar{p}$ (lower panels) compared to hydrodynamical calculations from the MUSIC model using IP-Glasma initial conditions (magenta) [82], the iEBE-VISHNU hybrid model using AMPT (orange) or T_RENTo (cyan) initial conditions [83]. Statistical and systematic uncertainties of the data points are shown as bars and boxes, respectively.
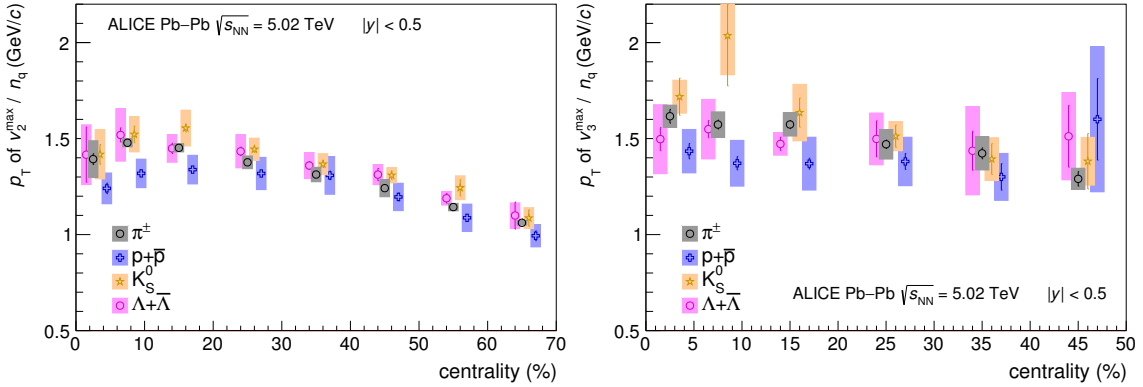

Figure 18. (Colour online) Centrality dependence of $p_T|_{v_2^{\max}}/n_q$ (left) and $p_T|_{v_3^{\max}}/n_q$ (right) divided by number of constituent quarks, n_q, for $\pi^\pm$, $p+\bar{p}$, $\Lambda+\bar{\Lambda}$, and K_S^0. Points are slightly shifted along the horizontal axis for better visibility in both panels. Statistical and systematic uncertainties are shown as bars and boxes, respectively.

$p+\bar{p}$ $p_T|_{v_2^{\max}}/n_q$, which is slightly lower in the 0–20% centrality range. The right panel of figure 18 presents $p_T|_{v_3^{\max}}/n_q$, which shows, within the large uncertainties, a weak (if any) centrality dependence for $\pi^\pm$ and K_S^0 and no centrality dependence for $p+\bar{p}$ and $\Lambda+\bar{\Lambda}$. The $p_T|_{v_3^{\max}}/n_q$ is the same for the different particle species within uncertainties.
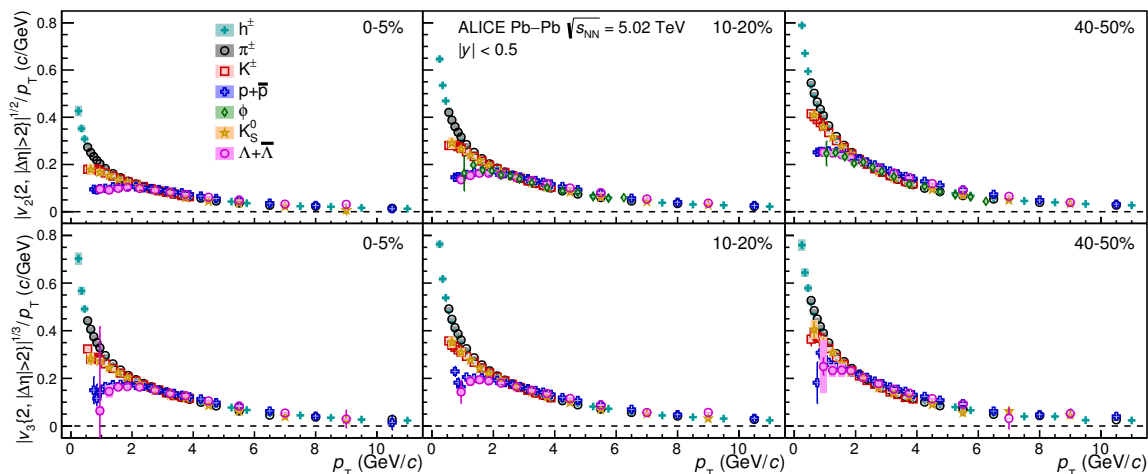
Figure 19. (Colour online) Centrality dependence of $|v_n|^{1/n}/p_T$ of inclusive charged particles [44], $\pi^\pm$, $K^\pm$, p+$\overline{p}$, Λ+$\overline{\Lambda}$, K_S^0, and the ϕ-meson for $n = 2$ (upper panels) and $n = 3$ (lower panels). Statistical and systematic uncertainties are shown as bars and boxes, respectively.

In the scenario of ideal hydrodynamics, v_n is a power law function of the radial expansion velocity of the medium [95, 96] so that $v_n \propto p_T^n$ up to $p_T \sim M$ for particles with mass M. Figure 19 shows $|v_n|^{1/n}/p_T$ as function of p_T for $n = 2$ and $n = 3$ in various centrality intervals for inclusive charged particles [44], $\pi^\pm$, $K^\pm$, p+$\overline{p}$, Λ+$\overline{\Lambda}$, K_S^0, and the ϕ-meson ($n = 2$ only). When $v_n \propto p_T^n$, the observable $|v_n|^{1/n}/p_T$ should be a constant. For $\pi^\pm$ and the inclusive charged particles, the $v_n \propto p_T^n$ scaling is broken both for v_2 and v_3 for all centrality intervals, as is also hypothesized in [97]. It should be noted however that the kinematic constraints imposed on the measurement preclude testing the scaling hypothesis in the full relevant momentum region. The scaling holds up to $p_T \approx 1\,\mathrm{GeV}/c$ for $K^\pm$ and K_S^0, and up to $p_T \approx 2\,\mathrm{GeV}/c$ for p+$\overline{p}$, Λ+$\overline{\Lambda}$, and the ϕ-meson for the 0–5% and 10–20% centrality intervals. Similar qualitative observations are found in the three hydrodynamical calculations [82, 83].

If v_n indeed exhibits a power law dependence on p_T^n, ratios of the form of $v_n^{1/n}/v_m^{1/m}$ are p_T-independent. Previous measurements at RHIC [98, 99] and the LHC [100, 101] have shown that the ratios $v_n^{1/n}/v_m^{1/m}$ show little to no p_T dependence up to about 6 GeV/c independent of the harmonic n and m for peripheral and semi-central collisions. However, a p_T dependence is observed for central collisions, which might be due to fluctuations in the initial geometry [99]. The ratios $v_3/|v_2|^{3/2}$, $v_4/|v_2|^{4/2}$, and $v_4/|v_3|^{4/3}$, which probe the same scaling but are in practice more sensitive, are shown in figures 20, 21, and 22, respectively. For each figure, $v_n/|v_m|^{n/m}$ is shown for inclusive charged particles [44], $\pi^\pm$, $K^\pm$ and p+$\overline{p}$ in various centrality intervals. For $v_3/|v_2|^{3/2}$ and $v_4/|v_2|^{4/2}$, no obvious p_T dependence is found for inclusive charged particles between 5–50% collision centrality. For the 0–5% centrality class, the ratios are flat for $p_T < 3$ GeV/c and rise monotonically for higher momenta. No particle type dependence of the ratios is found for $p_T > 1.5$ GeV/c, below which the ratios for p+$\overline{p}$ v_n rise. This rise of the p+$\overline{p}$ v_n ratios can be attributed to an increase of radial flow which affects the independent harmonics differently. For the ratio
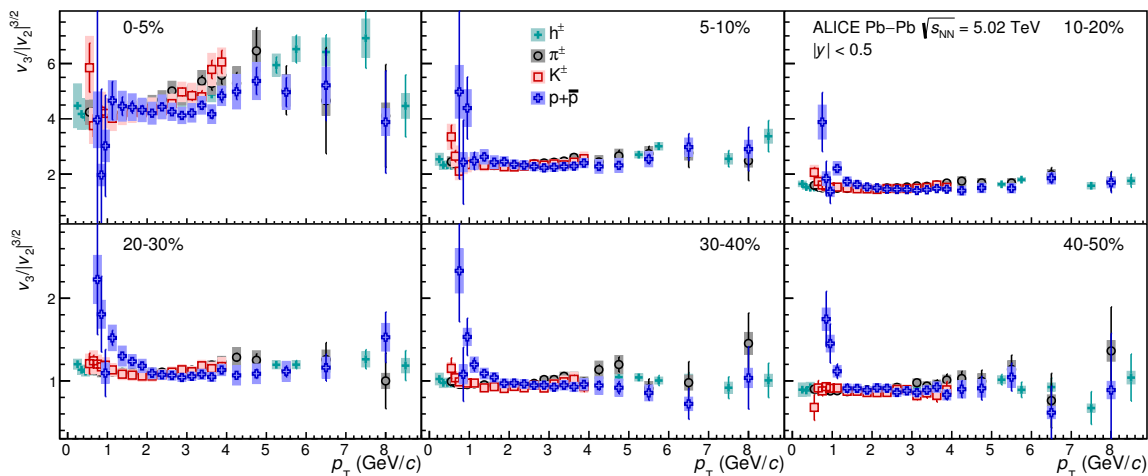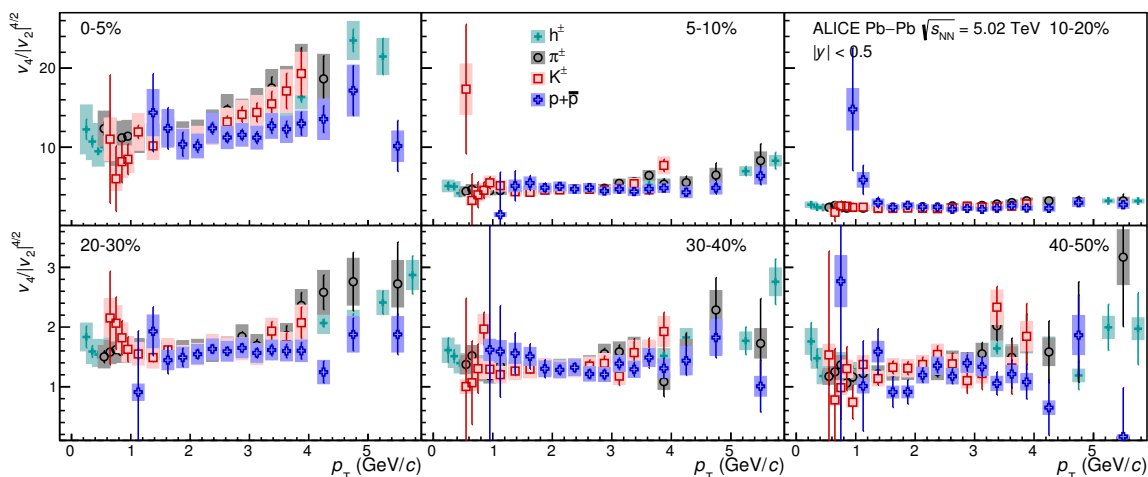
Figure 20. (Colour online) Centrality dependence of $v_3/|v_2|^{3/2}$ for inclusive charged particles [44], $\pi^\pm$, $K^\pm$, and p+$\overline{\text{p}}$. Statistical and systematic uncertainties are shown as bars and boxes, respectively.

Figure 21. (Colour online) Centrality dependence of $v_4/|v_2|^{4/2}$ for inclusive charged particles [44], $\pi^\pm$, $K^\pm$, and p+$\overline{\text{p}}$. Statistical and systematic uncertainties are shown as bars and boxes, respectively.

$v_4/|v_3|^{4/3}$, no p_{T} dependence is observed over the full centrality range. Large statistical uncertainties do not allow conclusions to be drawn on the behaviour of p+$\overline{\text{p}}$ v_n in the $v_4/|v_3|^{4/3}$ ratio.

4.5 Comparison with v_{n} of identified particles at $\sqrt{s_{\text{NN}}} = 2.76$ TeV

The transport properties and initial condition models can be further constrained by studying the energy dependence of anisotropic flow. Figure 23 presents the $v_2(p_{\text{T}})$, $v_3(p_{\text{T}})$, and $v_4(p_{\text{T}})$ of $\pi^\pm$, $K^\pm$, and p+$\overline{\text{p}}$ compared to ALICE measurements performed at $\sqrt{s_{\text{NN}}} = 2.76$ TeV [28].

The v_n coefficients at $\sqrt{s_{\text{NN}}} = 2.76$ TeV have been measured using the scalar product method, taking the particle of interest under study and the charged reference particles from different, non-overlapping pseudorapidity regions between $|\eta| < 0.8$. Assuming no
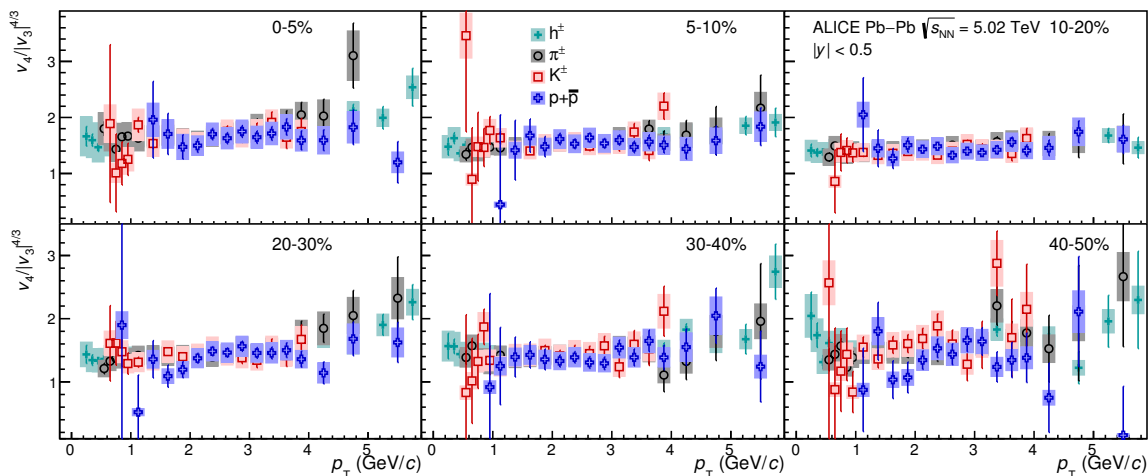
Figure 22. (Colour online) Centrality dependence of $v_4/|v_3|^{4/3}$ for inclusive charged particles [44], $\pi^\pm$, $K^\pm$, and p+$\overline{\text{p}}$. Statistical and systematic uncertainties are shown as bars and boxes, respectively.

anisotropic flow in minimum bias pp collisions at the same collision energy, the non-flow contributions are estimated from minimum bias pp collisions and subtracted from the measured v_n coefficients. Ratios of the measurements presented in this paper to a cubic spline fit to the ones performed at $\sqrt{s_{NN}} = 2.76$ TeV are given in the figure for each presented centrality interval and flow coefficient. The uncertainties in these ratios are obtained by summing the statistical and systematic uncertainties on the independent measurements in quadrature, and propagating the obtained uncertainties as uncorrelated.

An increase of radial flow with increasing collision energy is expected to lead to a suppression of v_n at low p_T, an effect which would be most pronounced for heavier particles. Although a possible suppression of p+$\overline{\text{p}}$ v_n at $\sqrt{s_{NN}} = 5.02$ TeV can be seen between $1 \lesssim p_T \lesssim 3$ GeV/c in central collisions and additionally for $v_2(p_T)$ of $\pi^\pm$ and $K^\pm$ at the same centrality interval, the precision of the results does not allow for conclusions to be drawn as the measurements at different collision energies are compatible within uncertainties.

Figure 24 shows the $v_2(p_T)$ of $\Lambda+\overline{\Lambda}$, K_S^0, and the ϕ-meson compared to ALICE measurements performed at $\sqrt{s_{NN}} = 2.76$ TeV [27], where the v_2 coefficients at $\sqrt{s_{NN}} = 2.76$ TeV have been measured using the scalar product method with an $|\Delta\eta| > 0.9$ gap to suppress non-flow. No differences are observed between the K_S^0 and $\Lambda+\overline{\Lambda}$ $v_2(p_T)$ measured at two different collision energies. The strongly improved precision of the ϕ-meson measurement at $\sqrt{s_{NN}} = 5.02$ TeV, both in terms of statistical uncertainty and granularity in p_T, shows that the $v_2(p_T)$ follows a mass ordering at low p_T and groups with mesons after $p_T \approx 3$ GeV/c for all centrality intervals.

5   Summary

In summary, the elliptic, triangular, and quadrangular flow coefficients of $\pi^\pm$, $K^\pm$, p+$\overline{\text{p}}$, $\Lambda+\overline{\Lambda}$, K_S^0, and the ϕ-meson have been measured in Pb-Pb collisions at $\sqrt{s_{NN}} = 5.02$ TeV over a broad range of transverse momentum and in various centrality ranges. The preci-
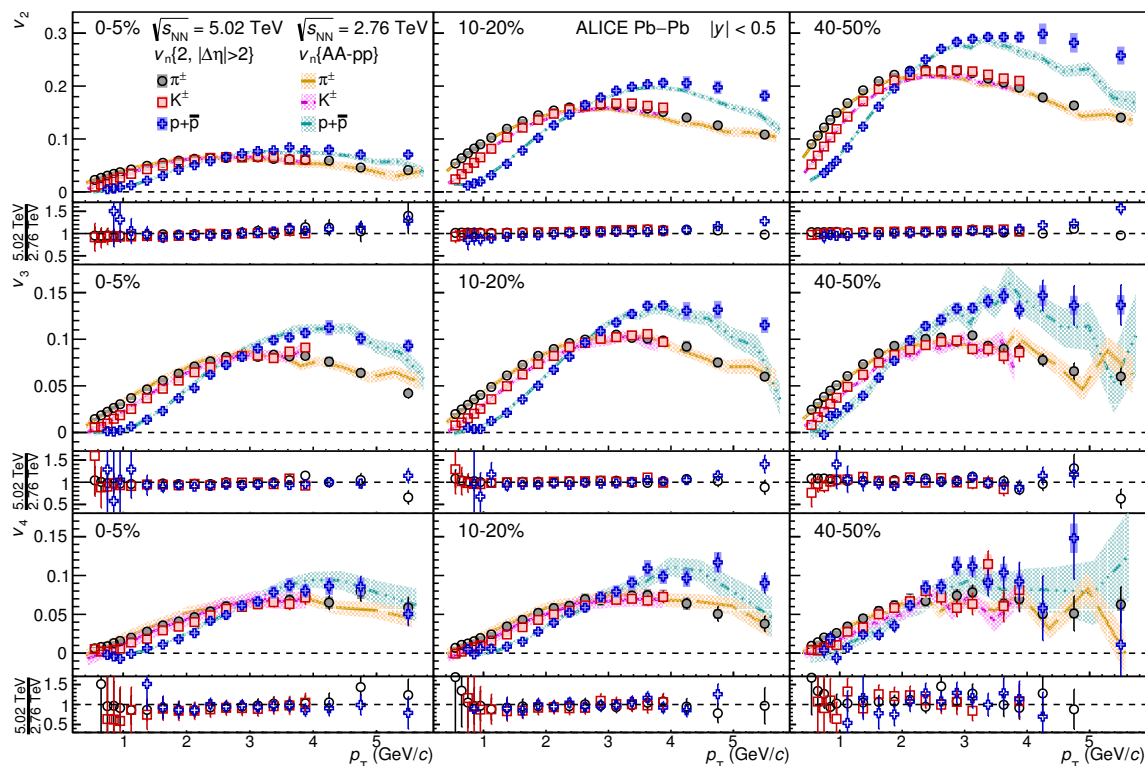
Figure 23. (Colour online) The p_T-differential v_2 (top), v_3 (middle), and v_4 (bottom) of $\pi^\pm$, $K^\pm$, and p+$\bar{\text{p}}$ compared to ALICE measurements performed in Pb-Pb collisions at $\sqrt{s_{NN}} = 2.76$ TeV (coloured bands) [28] for the 0–5%, 10–20%, and 40–50% centrality classes. For the measurements at $\sqrt{s_{NN}} = 5.02$ TeV, statistical and systematic uncertainties are shown as bars and boxes, respectively. For the measurements at $\sqrt{s_{NN}} = 2.76$ TeV, the thickness of the bands corresponds to the quadratic sum of statistical and systematic uncertainties. The ratios of measurements at $\sqrt{s_{NN}} = 5.02$ TeV to a cubic spline fit to the measurements at $\sqrt{s_{NN}} = 2.76$ TeV are also presented for clarity.

sion of these measurements provide constraints for initial-state fluctuations and transport coefficients of the medium. The magnitude of v_n increases with decreasing centrality up to the 40–50% centrality interval for all particle species. This increase is stronger for v_2 than for v_3 and v_4, which indicates that collision geometry dominates the generation of elliptic flow while higher flow coefficients are mainly generated by event-by-event fluctuations in the initial nucleon and gluon densities. This interpretation is also supported by the non-zero, positive v_n found in the 0–1% centrality interval. In most central collisions (i.e. 0–1% and 0–5%), v_3 and v_4 reach a similar magnitude as v_2 at different p_T values depending on particle mass, after which they increase gradually. For $p_T < 3$ GeV/c, the v_n coefficients show a mass ordering consistent with an interplay between anisotropic flow and the isotropic expansion (radial flow) of the collision system. In this transverse momentum range, the iEBE-VISHNU hydrodynamical calculations describe the measured v_n of $\pi^\pm$, $K^\pm$, and p+$\bar{\text{p}}$ fairly well for $p_T < 2.5$ GeV/c, while MUSIC reproduces the measurements for $p_T < 1$ GeV/c. It should be noted that neither of the presented hydrodynamical models is able to fully describe the measurements. At intermediate transverse momenta
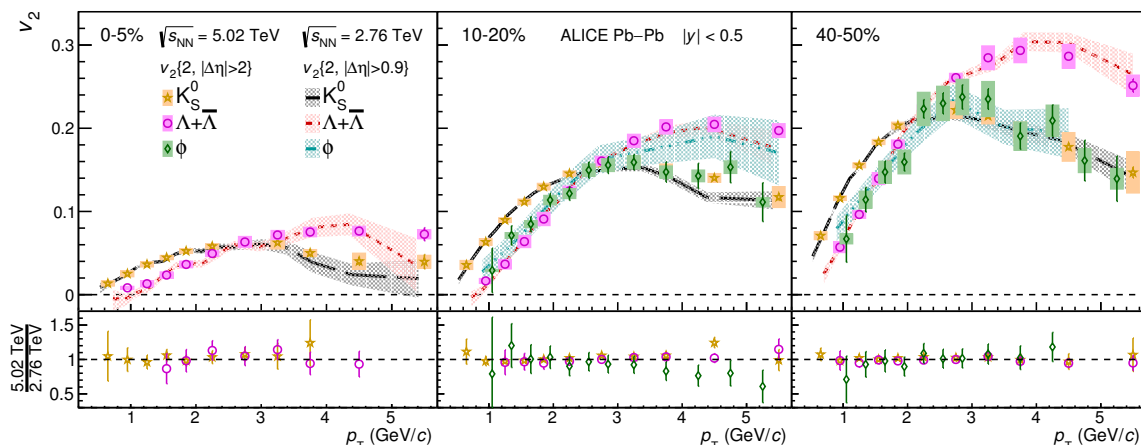
Figure 24. (Colour online) The p_T-differential v_2 of $\Lambda+\overline{\Lambda}$, K_S^0, and the ϕ-meson compared to AL-ICE measurements performed in Pb-Pb collisions at $\sqrt{s_{NN}} = 2.76\,\text{TeV}$ (coloured bands) [27] for the 0–5%, 10–20%, and 40–50% centrality classes. For the measurements at $\sqrt{s_{NN}} = 5.02\,\text{TeV}$, statistical and systematic uncertainties are shown as bars and boxes, respectively. For the measurements at $\sqrt{s_{NN}} = 2.76\,\text{TeV}$, the thickness of the bands corresponds to the quadratic sum of statistical and systematic uncertainties. The ratios of measurements at $\sqrt{s_{NN}} = 5.02\,\text{TeV}$ to a cubic spline fit to the measurements at $\sqrt{s_{NN}} = 2.76\,\text{TeV}$ are also presented for clarity.

$(3 < p_T < 8\text{–}10\,\text{GeV}/c)$, particles show an approximate grouping by the number of constituent quarks at the level of $\pm 20\%$ for all flow coefficients in the 0–50% centrality range. The ϕ-meson v_2, which tests both particle mass dependence and type scaling, follows p+$\overline{\text{p}}$ v_2 at low p_T and $\pi^{\pm}$ v_2 at intermediate p_T. The baryon v_n has a magnitude larger than that of mesons for $p_T < 8\text{–}10\,\text{GeV}/c$, indicating that the particle type dependence persists up to high p_T. For $p_T > 10\,\text{GeV}/c$, the v_2 of p+$\overline{\text{p}}$ is compatible with that of $\pi^{\pm}$ within uncertainties. The shape evolution of $v_2(p_T)$ as function of centrality shows different trends for $\pi^{\pm}$, $K^{\pm}$, and p+$\overline{\text{p}}$ and varies between 20% (10%) to 250% (55%) for p+$\overline{\text{p}}$ ($K^{\pm}$) at low p_T from most central to peripheral collisions; variations are more pronounced for $v_3(p_T)$, in particular for central collisions. Ratios $v_3/|v_2|^{3/2}$ and $v_4/|v_2|^{4/2}$ are flat for $p_T < 3\,\text{GeV}/c$ and rise monotonically for higher momenta for the 0–5% centrality class. No particle type dependence of the ratios is found for $p_T > 1.5\,\text{GeV}/c$, below which the ratios for p+$\overline{\text{p}}$ v_n rise, which can be attributed to an increase of radial flow which affects the independent harmonics differently. For the ratio $v_4/|v_3|^{4/3}$, no p_T dependence is observed over the full centrality range. The measurements are compatible with those performed in Pb-Pb collisions at $\sqrt{s_{NN}} = 2.76\,\text{TeV}$ within uncertainties.

Acknowledgments

References

[1] S.A. Bass, M. Gyulassy, H. Stoecker and W. Greiner, *Signatures of quark gluon plasma formation in high-energy heavy ion collisions: A Critical review*, *J. Phys.* **G 25** (1999) R1 [hep-ph/9810281] [INSPIRE].

[2] BRAHMS collaboration, I. Arsene et al., *Quark gluon plasma and color glass condensate at RHIC? The Perspective from the BRAHMS experiment*, *Nucl. Phys.* **A 757** (2005) 1 [nucl-ex/0410020] [INSPIRE].

[3] PHENIX collaboration, K. Adcox et al., *Formation of dense partonic matter in relativistic nucleus-nucleus collisions at RHIC: Experimental evaluation by the PHENIX collaboration*, *Nucl. Phys.* **A 757** (2005) 184 [nucl-ex/0410003] [INSPIRE].

[4] B.B. Back et al., *The PHOBOS perspective on discoveries at RHIC*, *Nucl. Phys.* **A 757** (2005) 28 [nucl-ex/0410022] [INSPIRE].

[5] STAR collaboration, J. Adams et al., *Experimental and theoretical challenges in the search for the quark gluon plasma: The STAR Collaboration's critical assessment of the evidence from RHIC collisions*, *Nucl. Phys.* **A 757** (2005) 102 [nucl-ex/0501009] [INSPIRE].

[6] ALICE collaboration, *Elliptic flow of charged particles in Pb-Pb collisions at 2.76 TeV*, *Phys. Rev. Lett.* **105** (2010) 252302 [arXiv:1011.3914] [INSPIRE].

[7] ATLAS collaboration, *Measurement of the pseudorapidity and transverse momentum dependence of the elliptic flow of charged particles in lead-lead collisions at $\sqrt{s_{NN}} = 2.76$ TeV with the ATLAS detector*, *Phys. Lett.* **B 707** (2012) 330 [arXiv:1108.6018] [INSPIRE].

[8] CMS collaboration, *Measurement of the elliptic anisotropy of charged particles produced in PbPb collisions at $\sqrt{s_{NN}} = 2.76$ TeV*, *Phys. Rev.* **C 87** (2013) 014902 [arXiv:1204.1409] [INSPIRE].

[9] P. Kovtun, D.T. Son and A.O. Starinets, *Viscosity in strongly interacting quantum field theories from black hole physics*, *Phys. Rev. Lett.* **94** (2005) 111601 [hep-th/0405231] [INSPIRE].

[10] J.-Y. Ollitrault, *Anisotropy as a signature of transverse collective flow*, *Phys. Rev.* **D 46** (1992) 229 [INSPIRE].

[11] S. Voloshin and Y. Zhang, *Flow study in relativistic nuclear collisions by Fourier expansion of Azimuthal particle distributions*, *Z. Phys.* **C 70** (1996) 665 [hep-ph/9407282] [INSPIRE].

[12] R.S. Bhalerao and J.-Y. Ollitrault, *Eccentricity fluctuations and elliptic flow at RHIC*, *Phys. Lett.* **B 641** (2006) 260 [nucl-th/0607009] [INSPIRE].

[13] PHOBOS collaboration, B. Alver et al., *Importance of correlations and fluctuations on the initial source eccentricity in high-energy nucleus-nucleus collisions*, *Phys. Rev.* **C 77** (2008) 014906 [arXiv:0711.3724] [INSPIRE].

[14] B. Alver and G. Roland, *Collision geometry fluctuations and triangular flow in heavy-ion collisions*, *Phys. Rev.* **C 81** (2010) 054905 [*Erratum ibid.* **C 82** (2010) 039903] [arXiv:1003.0194] [INSPIRE].

[15] B.H. Alver, C. Gombeaud, M. Luzum and J.-Y. Ollitrault, *Triangular flow in hydrodynamics and transport theory*, *Phys. Rev.* **C 82** (2010) 034913 [arXiv:1007.5469] [INSPIRE].

[16] D. Teaney and L. Yan, *Non linearities in the harmonic spectrum of heavy ion collisions with ideal and viscous hydrodynamics*, *Phys. Rev.* **C 86** (2012) 044908 [arXiv:1206.1905] [INSPIRE].

[17] ALICE collaboration, *Linear and non-linear flow modes in Pb-Pb collisions at $\sqrt{s_{\rm NN}} = 2.76\,TeV$*, *Phys. Lett.* **B 773** (2017) 68 [arXiv:1705.04377] [INSPIRE].

[18] D. Teaney and L. Yan, *Triangularity and Dipole Asymmetry in Heavy Ion Collisions*, *Phys. Rev.* **C 83** (2011) 064904 [arXiv:1010.1876] [INSPIRE].

[19] G.-Y. Qin, H. Petersen, S.A. Bass and B. Müller, *Translation of collision geometry fluctuations into momentum anisotropies in relativistic heavy-ion collisions*, *Phys. Rev.* **C 82** (2010) 064903 [arXiv:1009.1847] [INSPIRE].

[20] P. Huovinen, P.F. Kolb, U.W. Heinz, P.V. Ruuskanen and S.A. Voloshin, *Radial and elliptic flow at RHIC: Further predictions*, *Phys. Lett.* **B 503** (2001) 58 [hep-ph/0101136] [INSPIRE].

[21] D. Teaney, J. Lauret and E.V. Shuryak, *Flow at the SPS and RHIC as a quark gluon plasma signature*, *Phys. Rev. Lett.* **86** (2001) 4783 [nucl-th/0011058] [INSPIRE].

[22] S.A. Voloshin, *Transverse radial expansion and directed flow*, *Phys. Rev.* **C 55** (1997) R1630 [nucl-th/9611038] [INSPIRE].

[23] C. Shen, U. Heinz, P. Huovinen and H. Song, *Radial and elliptic flow in Pb+Pb collisions at the Large Hadron Collider from viscous hydrodynamic*, *Phys. Rev.* **C 84** (2011) 044903 [arXiv:1105.3226] [INSPIRE].

[24] E877 collaboration, J. Barrette et al., *Proton and pion production relative to the reaction plane in Au + Au collisions at AGS energies*, *Phys. Rev.* **C 56** (1997) 3254 [nucl-ex/9707002] [INSPIRE].

[25] STAR collaboration, J. Adams et al., *Particle type dependence of azimuthal anisotropy and nuclear modification of particle production in Au + Au collisions at $\sqrt{s_{\rm NN}} = 200\,GeV$*, *Phys. Rev. Lett.* **92** (2004) 052302 [nucl-ex/0306007] [INSPIRE].

[26] PHENIX collaboration, S.S. Adler et al., *Elliptic flow of identified hadrons in Au+Au collisions at $\sqrt{s_{\rm NN}} = 200\,GeV$*, *Phys. Rev. Lett.* **91** (2003) 182301 [nucl-ex/0305013] [INSPIRE].

[27] ALICE collaboration, *Elliptic flow of identified hadrons in Pb-Pb collisions at* $\sqrt{s_{NN}} = 2.76\,TeV$, *JHEP* **06** (2015) 190 [arXiv:1405.4632] [INSPIRE].

[28] ALICE collaboration, *Higher harmonic flow coefficients of identified hadrons in Pb-Pb collisions at* $\sqrt{s_{NN}} = 2.76\,TeV$, *JHEP* **09** (2016) 164 [arXiv:1606.06057] [INSPIRE].

[29] STAR collaboration, B.I. Abelev et al., *Mass, quark-number and* $\sqrt{s_{NN}}$ *dependence of the second and fourth flow harmonics in ultra-relativistic nucleus-nucleus collisions*, *Phys. Rev.* **C 75** (2007) 054906 [nucl-ex/0701010] [INSPIRE].

[30] STAR collaboration, B.I. Abelev et al., *Partonic flow and phi-meson production in Au + Au collisions at* $\sqrt{s_{NN}} = 200\,GeV$, *Phys. Rev. Lett.* **99** (2007) 112301 [nucl-ex/0703033] [INSPIRE].

[31] PHENIX collaboration, A. Adare et al., *Scaling properties of azimuthal anisotropy in Au+Au and Cu+Cu collisions at* $\sqrt{s_{NN}} = 200\,GeV$, *Phys. Rev. Lett.* **98** (2007) 162301 [nucl-ex/0608033] [INSPIRE].

[32] PHENIX collaboration, A. Adare et al., *Deviation from quark-number scaling of the anisotropy parameter* v_2 *of pions, kaons and protons in Au+Au collisions at* $\sqrt{s_{NN}} = 200\,GeV$, *Phys. Rev.* **C 85** (2012) 064914 [arXiv:1203.2644] [INSPIRE].

[33] ALICE collaboration, *Anisotropic flow of charged hadrons, pions and (anti-)protons measured at high transverse momentum in Pb-Pb collisions at* $\sqrt{s_{NN}} = 2.76\,TeV$, *Phys. Lett.* **B 719** (2013) 18 [arXiv:1205.5761] [INSPIRE].

[34] D. Molnár and S.A. Voloshin, *Elliptic flow at large transverse momenta from quark coalescence*, *Phys. Rev. Lett.* **91** (2003) 092301 [nucl-th/0302014] [INSPIRE].

[35] H. Sato and K. Yazaki, *On the coalescence model for high-energy nuclear reactions*, *Phys. Lett.* **B 98** (1981) 153 [INSPIRE].

[36] C.B. Dover, U.W. Heinz, E. Schnedermann and J. Zimányi, *Relativistic coalescence model for high-energy nuclear collisions*, *Phys. Rev.* **C 44** (1991) 1636 [INSPIRE].

[37] K. Werner, I. Karpenko, M. Bleicher, T. Pierog and S. Porteboeuf-Houssais, *Jets, Bulk Matter and their Interaction in Heavy Ion Collisions at Several TeV*, *Phys. Rev.* **C 85** (2012) 064907 [arXiv:1203.5704] [INSPIRE].

[38] K. Werner, *V2 Scaling in PbPb Collisions at* 2.76 *TeV*, arXiv:1205.3379 [INSPIRE].

[39] R. Baier, Y.L. Dokshitzer, S. Peigne and D. Schiff, *Induced gluon radiation in a QCD medium*, *Phys. Lett.* **B 345** (1995) 277 [hep-ph/9411409] [INSPIRE].

[40] M. Gyulassy and M. Plumer, *Jet Quenching in Dense Matter*, *Phys. Lett.* **B 243** (1990) 432 [INSPIRE].

[41] ATLAS collaboration, *Measurement of the Azimuthal Angle Dependence of Inclusive Jet Yields in Pb+Pb Collisions at* $\sqrt{s_{NN}} = 2.76\,TeV$ *with the ATLAS detector*, *Phys. Rev. Lett.* **111** (2013) 152301 [arXiv:1306.6469] [INSPIRE].

[42] ALICE collaboration, *Azimuthal anisotropy of charged jet production in* $\sqrt{s_{NN}} = 2.76\,TeV$ *Pb-Pb collisions*, *Phys. Lett.* **B 753** (2016) 511 [arXiv:1509.07334] [INSPIRE].

[43] CMS collaboration, *Azimuthal anisotropy of charged particles with transverse momentum up to* 100 *GeV/c in PbPb collisions at* $\sqrt{s_{NN}} = 5.02\,TeV$, *Phys. Lett.* **B 776** (2018) 195 [arXiv:1702.00630] [INSPIRE].

[44] ALICE collaboration, *Energy dependence and fluctuations of anisotropic flow in Pb-Pb collisions at* $\sqrt{s_{\rm NN}} = 5.02$ *and* 2.76 *TeV*, *JHEP* **07** (2018) 103 [arXiv:1804.02944] [inSPIRE].

[45] T. Hirano, U.W. Heinz, D. Kharzeev, R. Lacey and Y. Nara, *Hadronic dissipative effects on elliptic flow in ultrarelativistic heavy-ion collisions*, *Phys. Lett.* **B 636** (2006) 299 [nucl-th/0511046] [inSPIRE].

[46] S. Takeuchi, K. Murase, T. Hirano, P. Huovinen and Y. Nara, *Effects of hadronic rescattering on multistrange hadrons in high-energy nuclear collisions*, *Phys. Rev.* **C 92** (2015) 044907 [arXiv:1505.05961] [inSPIRE].

[47] STAR collaboration, B.I. Abelev et al., *Measurements of φ-meson production in relativistic heavy-ion collisions at RHIC*, *Phys. Rev.* **C 79** (2009) 064903 [arXiv:0809.4737] [inSPIRE].

[48] A. Shor, *φ-meson production as a probe of the quark gluon plasma*, *Phys. Rev. Lett.* **54** (1985) 1122 [inSPIRE].

[49] K. Haglin, *Collision rates for ρ-, ω- and φ-mesons at nonzero temperature*, *Nucl. Phys.* **A 584** (1995) 719 [nucl-th/9410028] [inSPIRE].

[50] W. Smith and K.L. Haglin, *Collision broadening of the φ meson in baryon rich hadronic matter*, *Phys. Rev.* **C 57** (1998) 1449 [nucl-th/9710026] [inSPIRE].

[51] L. Álvarez-Ruso and V. Koch, *φ-meson propagation in a hot hadronic gas*, *Phys. Rev.* **C 65** (2002) 054901 [nucl-th/0201011] [inSPIRE].

[52] T. Ishikawa et al., *φ photo-production from Li, C, Al and Cu nuclei at* $E_\gamma = 1.5$–2.4 *GeV*, *Phys. Lett.* **B 608** (2005) 215 [nucl-ex/0411016] [inSPIRE].

[53] H.J. Behrend et al., *Photoproduction of φ-mesons at small t values*, *Phys. Lett.* **B 56** (1975) 408 [inSPIRE].

[54] P. Muhlich, T. Falter, C. Greiner, J. Lehr, M. Post and U. Mosel, *Photoproduction of φ-mesons from nuclei*, *Phys. Rev.* **C 67** (2003) 024605 [nucl-th/0210079] [inSPIRE].

[55] ALICE collaboration, $K^*(892)^0$ *and* $φ(1020)$ *production in Pb-Pb collisions at* $\sqrt{s_{\rm NN}} = 2.76$ *TeV*, *Phys. Rev.* **C 91** (2015) 024609 [arXiv:1404.0495] [inSPIRE].

[56] HADES collaboration, J. Adamczewski-Musch et al., *Deep sub-threshold φ production in Au+Au collisions*, *Phys. Lett.* **B 778** (2018) 403 [arXiv:1703.08418] [inSPIRE].

[57] STAR collaboration, C. Adler et al., *Elliptic flow from two and four particle correlations in Au+Au collisions at* $\sqrt{s_{\rm NN}} = 130$ *GeV*, *Phys. Rev.* **C 66** (2002) 034904 [nucl-ex/0206001] [inSPIRE].

[58] S.A. Voloshin, A.M. Poskanzer and R. Snellings, *Collective phenomena in non-central nuclear collisions*, *Landolt-Bornstein* **23** (2010) 293 [arXiv:0809.2949] [inSPIRE].

[59] M. Luzum and J.-Y. Ollitrault, *Eliminating experimental bias in anisotropic-flow measurements of high-energy nuclear collisions*, *Phys. Rev.* **C 87** (2013) 044907 [arXiv:1209.2323] [inSPIRE].

[60] ALICE collaboration, *ALICE: Physics performance report, volume I*, *J. Phys.* **G 30** (2004) 1517 [inSPIRE].

[61] ALICE collaboration, *ALICE: Physics performance report, volume II*, *J. Phys.* **G 32** (2006) 1295 [inSPIRE].

[62] ALICE collaboration, *The ALICE experiment at the CERN LHC*, 2008 *JINST* **3** S08002 [INSPIRE].

[63] ALICE collaboration, *Performance of the ALICE Experiment at the CERN LHC*, *Int. J. Mod. Phys.* **A 29** (2014) 1430044 [arXiv:1402.4476] [INSPIRE].

[64] ALICE collaboration, *Alignment of the ALICE Inner Tracking System with cosmic-ray tracks*, 2010 *JINST* **5** P03003 [arXiv:1001.0502] [INSPIRE].

[65] J. Alme et al., *The ALICE TPC, a large 3-dimensional tracking device with fast readout for ultra-high multiplicity events*, *Nucl. Instrum. Meth.* **A 622** (2010) 316 [arXiv:1001.1950] [INSPIRE].

[66] A. Akindinov et al., *Performance of the ALICE Time-Of-Flight detector at the LHC*, *Eur. Phys. J. Plus* **128** (2013) 44 [INSPIRE].

[67] ALICE collaboration, *Performance of the ALICE VZERO system*, 2013 *JINST* **8** P10016 [arXiv:1306.3130] [INSPIRE].

[68] M. Bondila et al., *ALICE T0 detector*, *IEEE Trans. Nucl. Sci.* **52** (2005) 1705.

[69] ALICE collaboration, *Centrality determination of Pb-Pb collisions at $\sqrt{s_{NN}} = 2.76\,TeV$ with ALICE*, *Phys. Rev.* **C 88** (2013) 044909 [arXiv:1301.4361] [INSPIRE].

[70] ALICE collaboration, *Centrality dependence of π, K, p production in Pb-Pb collisions at $\sqrt{s_{NN}} = 2.76\,TeV$*, *Phys. Rev.* **C 88** (2013) 044910 [arXiv:1303.0737] [INSPIRE].

[71] PARTICLE DATA GROUP collaboration, C. Patrignani et al., *Review of Particle Physics*, *Chin. Phys.* **C 40** (2016) 100001 [INSPIRE].

[72] J. Podolanski and R. Armenteros, *III. Analysis of V-events*, *Philos. Mag.* **45** (1954) 13.

[73] G.I. Kopylov, *Like particle correlations as a tool to study the multiple production mechanism*, *Phys. Lett.* **B 50** (1974) 472 [INSPIRE].

[74] I. Selyuzhenkov and S. Voloshin, *Effects of non-uniform acceptance in anisotropic flow measurement*, *Phys. Rev.* **C 77** (2008) 034904 [arXiv:0707.4672] [INSPIRE].

[75] N. Borghini and J.Y. Ollitrault, *Azimuthally sensitive correlations in nucleus-nucleus collisions*, *Phys. Rev.* **C 70** (2004) 064905 [nucl-th/0407041] [INSPIRE].

[76] R. Barlow, *Systematic errors: Facts and fictions*, in *Advanced Statistical Techniques in Particle Physics. Proceedings, Conference*, Durham, U.K., March 18–22, 2002, pp. 134–144 (2002) [hep-ex/0207026] [INSPIRE].

[77] F.G. Gardim, F. Grassi, M. Luzum and J.-Y. Ollitrault, *Mapping the hydrodynamic response to the initial geometry in heavy-ion collisions*, *Phys. Rev.* **C 85** (2012) 024908 [arXiv:1111.6538] [INSPIRE].

[78] H. Song and U.W. Heinz, *Suppression of elliptic flow in a minimally viscous quark-gluon plasma*, *Phys. Lett.* **B 658** (2008) 279 [arXiv:0709.0742] [INSPIRE].

[79] H. Song, S. Bass and U.W. Heinz, *Spectra and elliptic flow for identified hadrons in 2.76A TeV Pb + Pb collisions*, *Phys. Rev.* **C 89** (2014) 034919 [arXiv:1311.0157] [INSPIRE].

[80] ALICE collaboration, *Centrality dependence of the nuclear modification factor of charged pions, kaons and protons in Pb-Pb collisions at $\sqrt{s_{NN}} = 2.76\,TeV$*, *Phys. Rev.* **C 93** (2016) 034913 [arXiv:1506.07287] [INSPIRE].

[81] V. Greco, C.M. Ko and P. Levai, *Parton coalescence at RHIC*, *Phys. Rev.* **C 68** (2003) 034904 [nucl-th/0305024] [INSPIRE].

[82] S. McDonald, C. Shen, F. Fillion-Gourdeau, S. Jeon and C. Gale, *Hydrodynamic predictions for Pb+Pb collisions at* 5.02 *TeV*, *Phys. Rev.* **C 95** (2017) 064913 [arXiv:1609.02958] [INSPIRE].

[83] W. Zhao, H.-j. Xu and H. Song, *Collective flow in* 2.76 *A TeV and* 5.02 *A TeV Pb+Pb collisions*, *Eur. Phys. J.* **C 77** (2017) 645 [arXiv:1703.10792] [INSPIRE].

[84] B. Schenke, S. Jeon and C. Gale, *Elliptic and triangular flow in event-by-event (3+1)D viscous hydrodynamics*, *Phys. Rev. Lett.* **106** (2011) 042301 [arXiv:1009.3244] [INSPIRE].

[85] S.A. Bass et al., *Microscopic models for ultrarelativistic heavy ion collisions*, *Prog. Part. Nucl. Phys.* **41** (1998) 255 [nucl-th/9803035] [INSPIRE].

[86] M. Bleicher et al., *Relativistic hadron hadron collisions in the ultrarelativistic quantum molecular dynamics model*, *J. Phys.* **G 25** (1999) 1859 [hep-ph/9909407] [INSPIRE].

[87] B. Schenke, P. Tribedy and R. Venugopalan, *Event-by-event gluon multiplicity, energy density and eccentricities in ultrarelativistic heavy-ion collisions*, *Phys. Rev.* **C 86** (2012) 034908 [arXiv:1206.6805] [INSPIRE].

[88] B. Schenke, P. Tribedy and R. Venugopalan, *Fluctuating Glasma initial conditions and flow in heavy ion collisions*, *Phys. Rev. Lett.* **108** (2012) 252301 [arXiv:1202.6646] [INSPIRE].

[89] C. Shen, Z. Qiu, H. Song, J. Bernhard, S. Bass and U. Heinz, *The iEBE-VISHNU code package for relativistic heavy-ion collisions*, *Comput. Phys. Commun.* **199** (2016) 61 [arXiv:1409.8164] [INSPIRE].

[90] H. Song, S.A. Bass and U. Heinz, *Viscous QCD matter in a hybrid hydrodynamic+Boltzmann approach*, *Phys. Rev.* **C 83** (2011) 024912 [arXiv:1012.0555] [INSPIRE].

[91] J.S. Moreland, J.E. Bernhard and S.A. Bass, *Alternative ansatz to wounded nucleon and binary collision scaling in high-energy nuclear collisions*, *Phys. Rev.* **C 92** (2015) 011901 [arXiv:1412.4708] [INSPIRE].

[92] Z.-W. Lin, C.M. Ko, B.-A. Li, B. Zhang and S. Pal, *A Multi-phase transport model for relativistic heavy ion collisions*, *Phys. Rev.* **C 72** (2005) 064901 [nucl-th/0411110] [INSPIRE].

[93] J.E. Bernhard, J.S. Moreland, S.A. Bass, J. Liu and U. Heinz, *Applying Bayesian parameter estimation to relativistic heavy-ion collisions: simultaneous characterization of the initial state and quark-gluon plasma medium*, *Phys. Rev.* **C 94** (2016) 024907 [arXiv:1605.03954] [INSPIRE].

[94] R.J. Fries, V. Greco and P. Sorensen, *Coalescence Models For Hadron Formation From Quark Gluon Plasma*, *Ann. Rev. Nucl. Part. Sci.* **58** (2008) 177 [arXiv:0807.4939] [INSPIRE].

[95] P.M. Dinh, N. Borghini and J.-Y. Ollitrault, *Effects of HBT correlations on flow measurements*, *Phys. Lett.* **B 477** (2000) 51 [nucl-th/9912013] [INSPIRE].

[96] N. Borghini and J.-Y. Ollitrault, *Momentum spectra, anisotropic flow and ideal fluids*, *Phys. Lett.* **B 642** (2006) 227 [nucl-th/0506045] [INSPIRE].

[97] B.H. Alver, C. Gombeaud, M. Luzum and J.-Y. Ollitrault, *Triangular flow in hydrodynamics and transport theory*, *Phys. Rev.* **C 82** (2010) 034913 [`arXiv:1007.5469`] [inSPIRE].

[98] STAR collaboration, J. Adams et al., *Azimuthal anisotropy at RHIC: The First and fourth harmonics*, *Phys. Rev. Lett.* **92** (2004) 062301 [`nucl-ex/0310029`] [inSPIRE].

[99] PHENIX collaboration, A. Adare et al., *Elliptic and hexadecapole flow of charged hadrons in Au+Au collisions at $\sqrt{s_{NN}} = 200\,GeV$*, *Phys. Rev. Lett.* **105** (2010) 062301 [`arXiv:1003.5586`] [inSPIRE].

[100] ATLAS collaboration, *Measurement of the azimuthal anisotropy for charged particle production in $\sqrt{s_{NN}} = 2.76\,TeV$ lead-lead collisions with the ATLAS detector*, *Phys. Rev.* **C 86** (2012) 014907 [`arXiv:1203.3087`] [inSPIRE].

[101] CMS collaboration, *Studies of azimuthal dihadron correlations in ultra-central PbPb collisions at $\sqrt{s_{NN}} = 2.76\,TeV$*, *JHEP* **02** (2014) 088 [`arXiv:1312.1845`] [inSPIRE].

The ALICE collaboration

S. Acharya[139] , F.T.-. Acosta[22] , D. Adamová[94] , J. Adolfsson[81] , M.M. Aggarwal[98] , G. Aglieri Rinella[36] , M. Agnello[33] , N. Agrawal[49] , Z. Ahammed[139] , S.U. Ahn[77] , S. Aiola[144] , A. Akindinov[65] , M. Al-Turany[104] , S.N. Alam[139] , D.S.D. Albuquerque[120] , D. Aleksandrov[88] , B. Alessandro[59] , R. Alfaro Molina[73] , Y. Ali[16] , A. Alici[11 ,54 ,29] , A. Alkin[3] , J. Alme[24] , T. Alt[70] , L. Altenkamper[24] , I. Altsybeev[138] , M.N. Anaam[7] , C. Andrei[48] , D. Andreou[36] , H.A. Andrews[108] , A. Andronic[142 ,104] , M. Angeletti[36] , V. Anguelov[102] , C. Anson[17] , T. Antičić[105] , F. Antinori[57] , P. Antonioli[54] , R. Anwar[124] , N. Apadula[80] , L. Aphecetche[112] , H. Appelshäuser[70] , S. Arcelli[29] , R. Arnaldi[59] , O.W. Arnold[103 ,115] , I.C. Arsene[23] , M. Arslandok[102] , B. Audurier[112] , A. Augustinus[36] , R. Averbeck[104] , M.D. Azmi[18] , A. Badalà[56] , Y.W. Baek[61 ,42] , S. Bagnasco[59] , R. Bailhache[70] , R. Bala[99] , A. Baldisseri[134] , M. Ball[44] , R.C. Baral[86] , A.M. Barbano[28] , R. Barbera[30] , F. Barile[53] , L. Barioglio[28] , G.G. Barnaföldi[143] , L.S. Barnby[93] , V. Barret[131] , P. Bartalini[7] , K. Barth[36] , E. Bartsch[70] , N. Bastid[131] , S. Basu[141] , G. Batigne[112] , B. Batyunya[76] , P.C. Batzing[23] , J.L. Bazo Alba[109] , I.G. Bearden[89] , H. Beck[102] , C. Bedda[64] , N.K. Behera[61] , I. Belikov[133] , F. Bellini[36] , H. Bello Martinez[2] , R. Bellwied[124] , L.G.E. Beltran[118] , V. Belyaev[92] , G. Bencedi[143] , S. Beole[28] , A. Bercuci[48] , Y. Berdnikov[96] , D. Berenyi[143] , R.A. Bertens[127] , D. Berzano[36 ,59] , L. Betev[36] , P.P. Bhaduri[139] , A. Bhasin[99] , I.R. Bhat[99] , H. Bhatt[49] , B. Bhattacharjee[43] , J. Bhom[116] , A. Bianchi[28] , L. Bianchi[124] , N. Bianchi[52] , J. Bielčík[39] , J. Bielčíková[94] , A. Bilandzic[115 ,103] , G. Biro[143] , R. Biswas[4] , S. Biswas[4] , J.T. Blair[117] , D. Blau[88] , C. Blume[70] , G. Boca[136] , F. Bock[36] , A. Bogdanov[92] , L. Boldizsár[143] , M. Bombara[40] , G. Bonomi[137] , M. Bonora[36] , H. Borel[134] , A. Borissov[20 ,142] , M. Borri[126] , E. Botta[28] , C. Bourjau[89] , L. Bratrud[70] , P. Braun-Munzinger[104] , M. Bregant[119] , T.A. Broker[70] , M. Broz[39] , E.J. Brucken[45] , E. Bruna[59] , G.E. Bruno[36 ,35] , D. Budnikov[106] , H. Buesching[70] , S. Bufalino[33] , P. Buhler[111] , P. Buncic[36] , O. Busch[130 , i] , Z. Buthelezi[74] , J.B. Butt[16] , J.T. Buxton[19] , J. Cabala[114] , D. Caffarri[90] , H. Caines[144] , A. Caliva[104] , E. Calvo Villar[109] , R.S. Camacho[2] , P. Camerini[27] , A.A. Capon[111] , F. Carena[36] , W. Carena[36] , F. Carnesecchi[29 ,11] , J. Castillo Castellanos[134] , A.J. Castro[127] , E.A.R. Casula[55] , C. Ceballos Sanchez[9] , S. Chandra[139] , B. Chang[125] , W. Chang[7] , S. Chapeland[36] , M. Chartier[126] , S. Chattopadhyay[139] , S. Chattopadhyay[107] , A. Chauvin[103 ,115] , C. Cheshkov[132] , B. Cheynis[132] , V. Chibante Barroso[36] , D.D. Chinellato[120] , S. Cho[61] , P. Chochula[36] , T. Chowdhury[131] , P. Christakoglou[90] , C.H. Christensen[89] , P. Christiansen[81] , T. Chujo[130] , S.U. Chung[20] , C. Cicalo[55] , L. Cifarelli[11 ,29] , F. Cindolo[54] , J. Cleymans[123] , F. Colamaria[53] , D. Colella[66 ,36 ,53] , A. Collu[80] , M. Colocci[29] , M. Concas[59 , ii] , G. Conesa Balbastre[79] , Z. Conesa del Valle[62] , J.G. Contreras[39] , T.M. Cormier[95] , Y. Corrales Morales[59] , P. Cortese[34] , M.R. Cosentino[121] , F. Costa[36] , S. Costanza[136] , J. Crkovská[62] , P. Crochet[131] , E. Cuautle[71] , L. Cunqueiro[142 ,95] , T. Dahms[103 ,115] , A. Dainese[57] , S. Dani[67] , M.C. Danisch[102] , A. Danu[69] , D. Das[107] , I. Das[107] , S. Das[4] , A. Dash[86] , S. Dash[49] , S. De[50] , A. De Caro[32] , G. de Cataldo[53] , C. de Conti[119] , J. de Cuveland[41] , A. De Falco[26] , D. De Gruttola[11 ,32] , N. De Marco[59] , S. De Pasquale[32] , R.D. De Souza[120] , H.F. Degenhardt[119] , A. Deisting[104 ,102] , A. Deloff[85] , S. Delsanto[28] , C. Deplano[90] , P. Dhankher[49] , D. Di Bari[35] , A. Di Mauro[36] , B. Di Ruzza[57] , R.A. Diaz[9] , T. Dietel[123] , P. Dillenseger[70] , Y. Ding[7] , R. Divià[36] , Ø. Djuvsland[24] , A. Dobrin[36] , D. Domenicis Gimenez[119] , B. Dönigus[70] , O. Dordic[23] , L.V.R. Doremalen[64] , A.K. Dubey[139] , A. Dubla[104] , L. Ducroux[132] , S. Dudi[98] , A.K. Duggal[98] , M. Dukhishyam[86] , P. Dupieux[131] , R.J. Ehlers[144] , D. Elia[53] , E. Endress[109] , H. Engel[75] , E. Epple[144] , B. Erazmus[112] , F. Erhardt[97] , M.R. Ersdal[24] , B. Espagnon[62] , G. Eulisse[36] , J. Eum[20] , D. Evans[108] , S. Evdokimov[91] , L. Fabbietti[103 ,115] , M. Faggin[31] , J. Faivre[79] , A. Fantoni[52] , M. Fasel[95] , L. Feldkamp[142] , A. Feliciello[59] , G. Feofilov[138] , A. Fernández Téllez[2] , A. Ferretti[28] ,

A. Festanti[31 ,36] , V.J.G. Feuillard[102] , J. Figiel[116] , M.A.S. Figueredo[119] , S. Filchagin[106] ,
D. Finogeev[63] , F.M. Fionda[24] , G. Fiorenza[53] , F. Flor[124] , M. Floris[36] , S. Foertsch[74] ,
P. Foka[104] , S. Fokin[88] , E. Fragiacomo[60] , A. Francescon[36] , A. Francisco[112] , U. Frankenfeld[104] ,
G.G. Fronze[28] , U. Fuchs[36] , C. Furget[79] , A. Furs[63] , M. Fusco Girard[32] , J.J. Gaardhøje[89] ,
M. Gagliardi[28] , A.M. Gago[109] , K. Gajdosova[89] , M. Gallio[28] , C.D. Galvan[118] , P. Ganoti[84] ,
C. Garabatos[104] , E. Garcia-Solis[12] , K. Garg[30] , C. Gargiulo[36] , P. Gasik[115 ,103] , E.F. Gauger[117] ,
M.B. Gay Ducati[72] , M. Germain[112] , J. Ghosh[107] , P. Ghosh[139] , S.K. Ghosh[4] , P. Gianotti[52] ,
P. Giubellino[104 ,59] , P. Giubilato[31] , P. Glässel[102] , D.M. Goméz Coral[73] , A. Gomez Ramirez[75] ,
V. Gonzalez[104] , P. González-Zamora[2] , S. Gorbunov[41] , L. Görlich[116] , S. Gotovac[37] ,
V. Grabski[73] , L.K. Graczykowski[140] , K.L. Graham[108] , L. Greiner[80] , A. Grelli[64] , C. Grigoras[36] ,
V. Grigoriev[92] , A. Grigoryan[1] , S. Grigoryan[76] , J.M. Gronefeld[104] , F. Grosa[33] ,
J.F. Grosse-Oetringhaus[36] , R. Grosso[104] , R. Guernane[79] , B. Guerzoni[29] , M. Guittiere[112] ,
K. Gulbrandsen[89] , T. Gunji[129] , A. Gupta[99] , R. Gupta[99] , I.B. Guzman[2] , R. Haake[36] ,
M.K. Habib[104] , C. Hadjidakis[62] , H. Hamagaki[82] , G. Hamar[143] , M. Hamid[7] , J.C. Hamon[133] ,
R. Hannigan[117] , M.R. Haque[64] , J.W. Harris[144] , A. Harton[12] , H. Hassan[79] ,
D. Hatzifotiadou[54 ,11] , S. Hayashi[129] , S.T. Heckel[70] , E. Hellbär[70] , H. Helstrup[38] ,
A. Herghelegiu[48] , E.G. Hernandez[2] , G. Herrera Corral[10] , F. Herrmann[142] , K.F. Hetland[38] ,
T.E. Hilden[45] , H. Hillemanns[36] , C. Hills[126] , B. Hippolyte[133] , B. Hohlweger[103] , D. Horak[39] ,
S. Hornung[104] , R. Hosokawa[130 ,79] , J. Hota[67] , P. Hristov[36] , C. Huang[62] , C. Hughes[127] ,
P. Huhn[70] , T.J. Humanic[19] , H. Hushnud[107] , N. Hussain[43] , T. Hussain[18] , D. Hutter[41] ,
D.S. Hwang[21] , J.P. Iddon[126] , S.A. Iga Buitron[71] , R. Ilkaev[106] , M. Inaba[130] , M. Ippolitov[88] ,
M.S. Islam[107] , M. Ivanov[104] , V. Ivanov[96] , V. Izucheev[91] , B. Jacak[80] , N. Jacazio[29] ,
P.M. Jacobs[80] , M.B. Jadhav[49] , S. Jadlovska[114] , J. Jadlovsky[114] , S. Jaelani[64] ,
C. Jahnke[119 ,115] , M.J. Jakubowska[140] , M.A. Janik[140] , C. Jena[86] , M. Jercic[97] , O. Jevons[108] ,
R.T. Jimenez Bustamante[104] , M. Jin[124] , P.G. Jones[108] , A. Jusko[108] , P. Kalinak[66] ,
A. Kalweit[36] , J.H. Kang[145] , V. Kaplin[92] , S. Kar[7] , A. Karasu Uysal[78] , O. Karavichev[63] ,
T. Karavicheva[63] , P. Karczmarczyk[36] , E. Karpechev[63] , U. Kebschull[75] , R. Keidel[47] ,
D.L.D. Keijdener[64] , M. Keil[36] , B. Ketzer[44] , Z. Khabanova[90] , A.M. Khan[7] , S. Khan[18] ,
S.A. Khan[139] , A. Khanzadeev[96] , Y. Kharlov[91] , A. Khatun[18] , A. Khuntia[50] ,
M.M. Kielbowicz[116] , B. Kileng[38] , B. Kim[130] , D. Kim[145] , D.J. Kim[125] , E.J. Kim[14] , H. Kim[145] ,
J.S. Kim[42] , J. Kim[102] , M. Kim[61 ,102] , S. Kim[21] , T. Kim[145] , T. Kim[145] , S. Kirsch[41] ,
I. Kisel[41] , S. Kiselev[65] , A. Kisiel[140] , J.L. Klay[6] , C. Klein[70] , J. Klein[36 ,59] , C. Klein-Bösing[142] ,
S. Klewin[102] , A. Kluge[36] , M.L. Knichel[36] , A.G. Knospe[124] , C. Kobdaj[113] , M. Kofarago[143] ,
M.K. Köhler[102] , T. Kollegger[104] , N. Kondratyeva[92] , E. Kondratyuk[91] , A. Konevskikh[63] ,
M. Konyushikhin[141] , O. Kovalenko[85] , V. Kovalenko[138] , M. Kowalski[116] , I. Králik[66] ,
A. Kravčáková[40] , L. Kreis[104] , M. Krivda[66 ,108] , F. Krizek[94] , M. Krüger[70] , E. Kryshen[96] ,
M. Krzewicki[41] , A.M. Kubera[19] , V. Kučera[94 ,61] , C. Kuhn[133] , P.G. Kuijer[90] , J. Kumar[49] ,
L. Kumar[98] , S. Kumar[49] , S. Kundu[86] , P. Kurashvili[85] , A. Kurepin[63] , A.B. Kurepin[63] ,
A. Kuryakin[106] , S. Kushpil[94] , J. Kvapil[108] , M.J. Kweon[61] , Y. Kwon[145] , S.L. La Pointe[41] ,
P. La Rocca[30] , Y.S. Lai[80] , I. Lakomov[36] , R. Langoy[122] , K. Lapidus[144] , A. Lardeux[23] ,
P. Larionov[52] , E. Laudi[36] , R. Lavicka[39] , R. Lea[27] , L. Leardini[102] , S. Lee[145] , F. Lehas[90] ,
S. Lehner[111] , J. Lehrbach[41] , R.C. Lemmon[93] , I. León Monzón[118] , P. Lévai[143] , X. Li[13] ,
X.L. Li[7] , J. Lien[122] , R. Lietava[108] , B. Lim[20] , S. Lindal[23] , V. Lindenstruth[41] , S.W. Lindsay[126] ,
C. Lippmann[104] , M.A. Lisa[19] , V. Litichevskyi[45] , A. Liu[80] , H.M. Ljunggren[81] , W.J. Llope[141] ,
D.F. Lodato[64] , V. Loginov[92] , C. Loizides[95 ,80] , P. Loncar[37] , X. Lopez[131] , E. López Torres[9] ,
A. Lowe[143] , P. Luettig[70] , J.R. Luhder[142] , M. Lunardon[31] , G. Luparello[60] , M. Lupi[36] ,
A. Maevskaya[63] , M. Mager[36] , S.M. Mahmood[23] , A. Maire[133] , R.D. Majka[144] , M. Malaev[96] ,
Q.W. Malik[23] , L. Malinina[76 , iii] , D. Mal'Kevich[65] , P. Malzacher[104] , A. Mamonov[106] ,

V. Manko[88] , F. Manso[131] , V. Manzari[53] , Y. Mao[7] , M. Marchisone[128 ,74 ,132] , J. Mareš[68] ,
G.V. Margagliotti[27] , A. Margotti[54] , J. Margutti[64] , A. Marín[104] , C. Markert[117] ,
M. Marquard[70] , N.A. Martin[104] , P. Martinengo[36] , J.L. Martinez[124] , M.I. Martínez[2] ,
G. Martínez García[112] , M. Martinez Pedreira[36] , S. Masciocchi[104] , M. Masera[28] , A. Masoni[55] ,
L. Massacrier[62] , E. Masson[112] , A. Mastroserio[53 ,135] , A.M. Mathis[115 ,103] , P.F.T. Matuoka[119] ,
A. Matyja[116 ,127] , C. Mayer[116] , M. Mazzilli[35] , M.A. Mazzoni[58] , F. Meddi[25] , Y. Melikyan[92] ,
A. Menchaca-Rocha[73] , E. Meninno[32] , J. Mercado Pérez[102] , M. Meres[15] , C.S. Meza[109] ,
S. Mhlanga[123] , Y. Miake[130] , L. Micheletti[28] , M.M. Mieskolainen[45] , D.L. Mihaylov[103] ,
K. Mikhaylov[65 ,76] , A. Mischke[64] , A.N. Mishra[71] , D. Miśkowiec[104] , J. Mitra[139] , C.M. Mitu[69] ,
N. Mohammadi[36] , A.P. Mohanty[64] , B. Mohanty[86] , M. Mohisin Khan[18 , iv] , D.A. Moreira De
Godoy[142] , L.A.P. Moreno[2] , S. Moretto[31] , A. Morreale[112] , A. Morsch[36] , V. Muccifora[52] ,
E. Mudnic[37] , D. Mühlheim[142] , S. Muhuri[139] , M. Mukherjee[4] , J.D. Mulligan[144] ,
M.G. Munhoz[119] , K. Münning[44] , M.I.A. Munoz[80] , R.H. Munzer[70] , H. Murakami[129] ,
S. Murray[74] , L. Musa[36] , J. Musinsky[66] , C.J. Myers[124] , J.W. Myrcha[140] , B. Naik[49] , R. Nair[85] ,
B.K. Nandi[49] , R. Nania[54 ,11] , E. Nappi[53] , A. Narayan[49] , M.U. Naru[16] , A.F. Nassirpour[81] ,
H. Natal da Luz[119] , C. Nattrass[127] , S.R. Navarro[2] , K. Nayak[86] , R. Nayak[49] , T.K. Nayak[139] ,
S. Nazarenko[106] , R.A. Negrao De Oliveira[70 ,36] , L. Nellen[71] , S.V. Nesbo[38] , G. Neskovic[41] ,
F. Ng[124] , M. Nicassio[104] , J. Niedziela[140 ,36] , B.S. Nielsen[89] , S. Nikolaev[88] , S. Nikulin[88] ,
V. Nikulin[96] , F. Noferini[11 ,54] , P. Nomokonov[76] , G. Nooren[64] , J.C.C. Noris[2] , J. Norman[79] ,
A. Nyanin[88] , J. Nystrand[24] , H. Oh[145] , A. Ohlson[102] , J. Oleniacz[140] , A.C. Oliveira Da Silva[119] ,
M.H. Oliver[144] , J. Onderwaater[104] , C. Oppedisano[59] , R. Orava[45] , M. Oravec[114] , A. Ortiz
Velasquez[71] , A. Oskarsson[81] , J. Otwinowski[116] , K. Oyama[82] , Y. Pachmayer[102] , V. Pacik[89] ,
D. Pagano[137] , G. Paić[71] , P. Palni[7] , J. Pan[141] , A.K. Pandey[49] , S. Panebianco[134] ,
V. Papikyan[1] , P. Pareek[50] , J. Park[61] , J.E. Parkkila[125] , S. Parmar[98] , A. Passfeld[142] ,
S.P. Pathak[124] , R.N. Patra[139] , B. Paul[59] , H. Pei[7] , T. Peitzmann[64] , X. Peng[7] , L.G. Pereira[72] ,
H. Pereira Da Costa[134] , D. Peresunko[88] , E. Perez Lezama[70] , V. Peskov[70] , Y. Pestov[5] ,
V. Petráček[39] , M. Petrovici[48] , C. Petta[30] , R.P. Pezzi[72] , S. Piano[60] , M. Pikna[15] , P. Pillot[112] ,
L.O.D.L. Pimentel[89] , O. Pinazza[54 ,36] , L. Pinsky[124] , S. Pisano[52] , D.B. Piyarathna[124] ,
M. Płoskoń[80] , M. Planinic[97] , F. Pliquett[70] , J. Pluta[140] , S. Pochybova[143] ,
P.L.M. Podesta-Lerma[118] , M.G. Poghosyan[95] , B. Polichtchouk[91] , N. Poljak[97] ,
W. Poonsawat[113] , A. Pop[48] , H. Poppenborg[142] , S. Porteboeuf-Houssais[131] , V. Pozdniakov[76] ,
S.K. Prasad[4] , R. Preghenella[54] , F. Prino[59] , C.A. Pruneau[141] , I. Pshenichnov[63] , M. Puccio[28] ,
V. Punin[106] , J. Putschke[141] , S. Raha[4] , S. Rajput[99] , J. Rak[125] , A. Rakotozafindrabe[134] ,
L. Ramello[34] , F. Rami[133] , R. Raniwala[100] , S. Raniwala[100] , S.S. Räsänen[45] , B.T. Rascanu[70] ,
V. Ratza[44] , I. Ravasenga[33] , K.F. Read[127 ,95] , K. Redlich[85 , v] , A. Rehman[24] , P. Reichelt[70] ,
F. Reidt[36] , X. Ren[7] , R. Renfordt[70] , A. Reshetin[63] , J.-P. Revol[11] , K. Reygers[102] , V. Riabov[96] ,
T. Richert[64 ,81] , M. Richter[23] , P. Riedler[36] , W. Riegler[36] , F. Riggi[30] , C. Ristea[69] ,
S.P. Rode[50] , M. Rodríguez Cahuantzi[2] , K. Røed[23] , R. Rogalev[91] , E. Rogochaya[76] , D. Rohr[36] ,
D. Röhrich[24] , P.S. Rokita[140] , F. Ronchetti[52] , E.D. Rosas[71] , K. Roslon[140] , P. Rosnet[131] ,
A. Rossi[31] , A. Rotondi[136] , F. Roukoutakis[84] , C. Roy[133] , P. Roy[107] , O.V. Rueda[71] , R. Rui[27] ,
B. Rumyantsev[76] , A. Rustamov[87] , E. Ryabinkin[88] , Y. Ryabov[96] , A. Rybicki[116] , S. Saarinen[45] ,
S. Sadhu[139] , S. Sadovsky[91] , K. Šafařík[36] , S.K. Saha[139] , B. Sahoo[49] , P. Sahoo[50] , R. Sahoo[50] ,
S. Sahoo[67] , P.K. Sahu[67] , J. Saini[139] , S. Sakai[130] , M.A. Saleh[141] , S. Sambyal[99] ,
V. Samsonov[96 ,92] , A. Sandoval[73] , A. Sarkar[74] , D. Sarkar[139] , N. Sarkar[139] , P. Sarma[43] ,
M.H.P. Sas[64] , E. Scapparone[54] , F. Scarlassara[31] , B. Schaefer[95] , H.S. Scheid[70] , C. Schiaua[48] ,
R. Schicker[102] , C. Schmidt[104] , H.R. Schmidt[101] , M.O. Schmidt[102] , M. Schmidt[101] ,
N.V. Schmidt[95 ,70] , J. Schukraft[36] , Y. Schutz[36 ,133] , K. Schwarz[104] , K. Schweda[104] ,
G. Scioli[29] , E. Scomparin[59] , M. Šefčík[40] , J.E. Seger[17] , Y. Sekiguchi[129] , D. Sekihata[46] ,

I. Selyuzhenkov[104],[92], K. Senosi[74], S. Senyukov[133], E. Serradilla[73], P. Sett[49], A. Sevcenco[69], A. Shabanov[63], A. Shabetai[112], R. Shahoyan[36], W. Shaikh[107], A. Shangaraev[91], A. Sharma[98], A. Sharma[99], M. Sharma[99], N. Sharma[98], A.I. Sheikh[139], K. Shigaki[46], M. Shimomura[83], S. Shirinkin[65], Q. Shou[7],[110], K. Shtejer[28], Y. Sibiriak[88], S. Siddhanta[55], K.M. Sielewicz[36], T. Siemiarczuk[85], D. Silvermyr[81], G. Simatovic[90], G. Simonetti[36],[103], R. Singaraju[139], R. Singh[86], R. Singh[99], V. Singhal[139], T. Sinha[107], B. Sitar[15], M. Sitta[34], T.B. Skaali[23], M. Slupecki[125], N. Smirnov[144], R.J.M. Snellings[64], T.W. Snellman[125], J. Song[20], F. Soramel[31], S. Sorensen[127], F. Sozzi[104], I. Sputowska[116], J. Stachel[102], I. Stan[69], P. Stankus[95], E. Stenlund[81], D. Stocco[112], M.M. Storetvedt[38], P. Strmen[15], A.A.P. Suaide[119], T. Sugitate[46], C. Suire[62], M. Suleymanov[16], M. Suljic[36],[27], R. Sultanov[65], M. Šumbera[94], S. Sumowidagdo[51], K. Suzuki[111], S. Swain[67], A. Szabo[15], I. Szarka[15], U. Tabassam[16], J. Takahashi[120], G.J. Tambave[24], N. Tanaka[130], M. Tarhini[112], M. Tariq[18], M.G. Tarzila[48], A. Tauro[36], G. Tejeda Muñoz[2], A. Telesca[36], C. Terrevoli[31], B. Teyssier[132], D. Thakur[50], S. Thakur[139], D. Thomas[117], F. Thoresen[89], R. Tieulent[132], A. Tikhonov[63], A.R. Timmins[124], A. Toia[70], N. Topilskaya[63], M. Toppi[52], S.R. Torres[118], S. Tripathy[50], S. Trogolo[28], G. Trombetta[35], L. Tropp[40], V. Trubnikov[3], W.H. Trzaska[125], T.P. Trzcinski[140], B.A. Trzeciak[64], T. Tsuji[129], A. Tumkin[106], R. Turrisi[57], T.S. Tveter[23], K. Ullaland[24], E.N. Umaka[124], A. Uras[132], G.L. Usai[26], A. Utrobicic[97], M. Vala[114], J.W. Van Hoorne[36], M. van Leeuwen[64], P. Vande Vyvre[36], D. Varga[143], A. Vargas[2], M. Vargyas[125], R. Varma[49], M. Vasileiou[84], A. Vasiliev[88], A. Vauthier[79], O. Vázquez Doce[103],[115], V. Vechernin[138], A.M. Veen[64], E. Vercellin[28], S. Vergara Limón[2], L. Vermunt[64], R. Vernet[8], R. Vértesi[143], L. Vickovic[37], J. Viinikainen[125], Z. Vilakazi[128], O. Villalobos Baillie[108], A. Villatoro Tello[2], A. Vinogradov[88], T. Virgili[32], V. Vislavicius[89],[81], A. Vodopyanov[76], M.A. Völkl[101], K. Voloshin[65], S.A. Voloshin[141], G. Volpe[35], B. von Haller[36], I. Vorobyev[115],[103], D. Voscek[114], D. Vranic[104],[36], J. Vrláková[40], B. Wagner[24], H. Wang[64], M. Wang[7], Y. Watanabe[130], M. Weber[111], S.G. Weber[104], A. Wegrzynek[36], D.F. Weiser[102], S.C. Wenzel[36], J.P. Wessels[142], U. Westerhoff[142], A.M. Whitehead[123], J. Wiechula[70], J. Wikne[23], G. Wilk[85], J. Wilkinson[54], G.A. Willems[142],[36], M.C.S. Williams[54], E. Willsher[108], B. Windelband[102], W.E. Witt[127], R. Xu[7], S. Yalcin[78], K. Yamakawa[46], S. Yano[46], Z. Yin[7], H. Yokoyama[79],[130], I.-K. Yoo[20], J.H. Yoon[61], V. Yurchenko[3], V. Zaccolo[59], A. Zaman[16], C. Zampolli[36], H.J.C. Zanoli[119], N. Zardoshti[108], A. Zarochentsev[138], P. Závada[68], N. Zaviyalov[106], H. Zbroszczyk[140], M. Zhalov[96], X. Zhang[7], Y. Zhang[7], Z. Zhang[7],[131], C. Zhao[23], V. Zherebchevskii[138], N. Zhigareva[65], D. Zhou[7], Y. Zhou[89], Z. Zhou[24], H. Zhu[7], J. Zhu[7], Y. Zhu[7], A. Zichichi[29],[11], M.B. Zimmermann[36], G. Zinovjev[3], J. Zmeskal[111], S. Zou[7]

[i] Deceased

[ii] Dipartimento DET del Politecnico di Torino, Turin, Italy

[iii] M.V. Lomonosov Moscow State University, D.V. Skobeltsyn Institute of Nuclear, Physics, Moscow, Russia

[iv] Department of Applied Physics, Aligarh Muslim University, Aligarh, India

[v] Institute of Theoretical Physics, University of Wroclaw, Poland

[1] A.I. Alikhanyan National Science Laboratory (Yerevan Physics Institute) Foundation, Yerevan, Armenia

[2] Benemérita Universidad Autónoma de Puebla, Puebla, Mexico

[3] Bogolyubov Institute for Theoretical Physics, National Academy of Sciences of Ukraine, Kiev, Ukraine

[4] Bose Institute, Department of Physics and Centre for Astroparticle Physics and Space Science (CAPSS), Kolkata, India

[5] Budker Institute for Nuclear Physics, Novosibirsk, Russia

[6] *California Polytechnic State University, San Luis Obispo, California, United States*

[7] *Central China Normal University, Wuhan, China*

[8] *Centre de Calcul de l'IN2P3, Villeurbanne, Lyon, France*

[9] *Centro de Aplicaciones Tecnológicas y Desarrollo Nuclear (CEADEN), Havana, Cuba*

[10] *Centro de Investigación y de Estudios Avanzados (CINVESTAV), Mexico City and Mérida, Mexico*

[11] *Centro Fermi - Museo Storico della Fisica e Centro Studi e Ricerche "Enrico Fermi", Rome, Italy*

[12] *Chicago State University, Chicago, Illinois, United States*

[13] *China Institute of Atomic Energy, Beijing, China*

[14] *Chonbuk National University, Jeonju, Republic of Korea*

[15] *Comenius University Bratislava, Faculty of Mathematics, Physics and Informatics, Bratislava, Slovakia*

[16] *COMSATS Institute of Information Technology (CIIT), Islamabad, Pakistan*

[17] *Creighton University, Omaha, Nebraska, United States*

[18] *Department of Physics, Aligarh Muslim University, Aligarh, India*

[19] *Department of Physics, Ohio State University, Columbus, Ohio, United States*

[20] *Department of Physics, Pusan National University, Pusan, Republic of Korea*

[21] *Department of Physics, Sejong University, Seoul, Republic of Korea*

[22] *Department of Physics, University of California, Berkeley, California, United States*

[23] *Department of Physics, University of Oslo, Oslo, Norway*

[24] *Department of Physics and Technology, University of Bergen, Bergen, Norway*

[25] *Dipartimento di Fisica dell'Università 'La Sapienza' and Sezione INFN, Rome, Italy*

[26] *Dipartimento di Fisica dell'Università and Sezione INFN, Cagliari, Italy*

[27] *Dipartimento di Fisica dell'Università and Sezione INFN, Trieste, Italy*

[28] *Dipartimento di Fisica dell'Università and Sezione INFN, Turin, Italy*

[29] *Dipartimento di Fisica e Astronomia dell'Università and Sezione INFN, Bologna, Italy*

[30] *Dipartimento di Fisica e Astronomia dell'Università and Sezione INFN, Catania, Italy*

[31] *Dipartimento di Fisica e Astronomia dell'Università and Sezione INFN, Padova, Italy*

[32] *Dipartimento di Fisica 'E.R. Caianiello' dell'Università and Gruppo Collegato INFN, Salerno, Italy*

[33] *Dipartimento DISAT del Politecnico and Sezione INFN, Turin, Italy*

[34] *Dipartimento di Scienze e Innovazione Tecnologica dell'Università del Piemonte Orientale and INFN Sezione di Torino, Alessandria, Italy*

[35] *Dipartimento Interateneo di Fisica 'M. Merlin' and Sezione INFN, Bari, Italy*

[36] *European Organization for Nuclear Research (CERN), Geneva, Switzerland*

[37] *Faculty of Electrical Engineering, Mechanical Engineering and Naval Architecture, University of Split, Split, Croatia*

[38] *Faculty of Engineering and Science, Western Norway University of Applied Sciences, Bergen, Norway*

[39] *Faculty of Nuclear Sciences and Physical Engineering, Czech Technical University in Prague, Prague, Czech Republic*

[40] *Faculty of Science, P.J. Šafárik University, Košice, Slovakia*

[41] *Frankfurt Institute for Advanced Studies, Johann Wolfgang Goethe-Universität Frankfurt, Frankfurt, Germany*

[42] *Gangneung-Wonju National University, Gangneung, Republic of Korea*

[43] *Gauhati University, Department of Physics, Guwahati, India*

[44] *Helmholtz-Institut für Strahlen- und Kernphysik, Rheinische Friedrich-Wilhelms-Universität Bonn, Bonn, Germany*

[45] *Helsinki Institute of Physics (HIP), Helsinki, Finland*

[46] *Hiroshima University, Hiroshima, Japan*

[47] *Hochschule Worms, Zentrum für Technologietransfer und Telekommunikation (ZTT), Worms, Germany*

[48] *Horia Hulubei National Institute of Physics and Nuclear Engineering, Bucharest, Romania*

[49] *Indian Institute of Technology Bombay (IIT), Mumbai, India*

50   *Indian Institute of Technology Indore, Indore, India*

51   *Indonesian Institute of Sciences, Jakarta, Indonesia*

52   *INFN, Laboratori Nazionali di Frascati, Frascati, Italy*

53   *INFN, Sezione di Bari, Bari, Italy*

54   *INFN, Sezione di Bologna, Bologna, Italy*

55   *INFN, Sezione di Cagliari, Cagliari, Italy*

56   *INFN, Sezione di Catania, Catania, Italy*

57   *INFN, Sezione di Padova, Padova, Italy*

58   *INFN, Sezione di Roma, Rome, Italy*

59   *INFN, Sezione di Torino, Turin, Italy*

60   *INFN, Sezione di Trieste, Trieste, Italy*

61   *Inha University, Incheon, Republic of Korea*

62   *Institut de Physique Nucléaire d'Orsay (IPNO), Institut National de Physique Nucléaire et de Physique des Particules (IN2P3/CNRS), Université de Paris-Sud, Université Paris-Saclay, Orsay, France*

63   *Institute for Nuclear Research, Academy of Sciences, Moscow, Russia*

64   *Institute for Subatomic Physics, Utrecht University/Nikhef, Utrecht, Netherlands*

65   *Institute for Theoretical and Experimental Physics, Moscow, Russia*

66   *Institute of Experimental Physics, Slovak Academy of Sciences, Košice, Slovakia*

67   *Institute of Physics, Bhubaneswar, India*

68   *Institute of Physics of the Czech Academy of Sciences, Prague, Czech Republic*

69   *Institute of Space Science (ISS), Bucharest, Romania*

70   *Institut für Kernphysik, Johann Wolfgang Goethe-Universität Frankfurt, Frankfurt, Germany*

71   *Instituto de Ciencias Nucleares, Universidad Nacional Autónoma de México, Mexico City, Mexico*

72   *Instituto de Física, Universidade Federal do Rio Grande do Sul (UFRGS), Porto Alegre, Brazil*

73   *Instituto de Física, Universidad Nacional Autónoma de México, Mexico City, Mexico*

74   *iThemba LABS, National Research Foundation, Somerset West, South Africa*

75   *Johann-Wolfgang-Goethe Universität Frankfurt Institut für Informatik, Fachbereich Informatik und Mathematik, Frankfurt, Germany*

76   *Joint Institute for Nuclear Research (JINR), Dubna, Russia*

77   *Korea Institute of Science and Technology Information, Daejeon, Republic of Korea*

78   *KTO Karatay University, Konya, Turkey*

79   *Laboratoire de Physique Subatomique et de Cosmologie, Université Grenoble-Alpes, CNRS-IN2P3, Grenoble, France*

80   *Lawrence Berkeley National Laboratory, Berkeley, California, United States*

81   *Lund University Department of Physics, Division of Particle Physics, Lund, Sweden*

82   *Nagasaki Institute of Applied Science, Nagasaki, Japan*

83   *Nara Women's University (NWU), Nara, Japan*

84   *National and Kapodistrian University of Athens, School of Science, Department of Physics, Athens, Greece*

85   *National Centre for Nuclear Research, Warsaw, Poland*

86   *National Institute of Science Education and Research, HBNI, Jatni, India*

87   *National Nuclear Research Center, Baku, Azerbaijan*

88   *National Research Centre Kurchatov Institute, Moscow, Russia*

89   *Niels Bohr Institute, University of Copenhagen, Copenhagen, Denmark*

90   *Nikhef, National institute for subatomic physics, Amsterdam, Netherlands*

91   *NRC Kurchatov Institute IHEP, Protvino, Russia*

92   *NRNU Moscow Engineering Physics Institute, Moscow, Russia*

93   *Nuclear Physics Group, STFC Daresbury Laboratory, Daresbury, United Kingdom*

94   *Nuclear Physics Institute of the Czech Academy of Sciences, Řež u Prahy, Czech Republic*

95   *Oak Ridge National Laboratory, Oak Ridge, Tennessee, United States*

96   *Petersburg Nuclear Physics Institute, Gatchina, Russia*

97 *Physics department, Faculty of science, University of Zagreb, Zagreb, Croatia*
98 *Physics Department, Panjab University, Chandigarh, India*
99 *Physics Department, University of Jammu, Jammu, India*
100 *Physics Department, University of Rajasthan, Jaipur, India*
101 *Physikalisches Institut, Eberhard-Karls-Universität Tübingen, Tübingen, Germany*
102 *Physikalisches Institut, Ruprecht-Karls-Universität Heidelberg, Heidelberg, Germany*
103 *Physik Department, Technische Universität München, Munich, Germany*
104 *Research Division and ExtreMe Matter Institute EMMI, GSI Helmholtzzentrum für Schwerionenforschung GmbH, Darmstadt, Germany*
105 *Rudjer Bošković Institute, Zagreb, Croatia*
106 *Russian Federal Nuclear Center (VNIIEF), Sarov, Russia*
107 *Saha Institute of Nuclear Physics, Kolkata, India*
108 *School of Physics and Astronomy, University of Birmingham, Birmingham, United Kingdom*
109 *Sección Física, Departamento de Ciencias, Pontificia Universidad Católica del Perú, Lima, Peru*
110 *Shanghai Institute of Applied Physics, Shanghai, China*
111 *Stefan Meyer Institut für Subatomare Physik (SMI), Vienna, Austria*
112 *SUBATECH, IMT Atlantique, Université de Nantes, CNRS-IN2P3, Nantes, France*
113 *Suranaree University of Technology, Nakhon Ratchasima, Thailand*
114 *Technical University of Košice, Košice, Slovakia*
115 *Technische Universität München, Excellence Cluster 'Universe', Munich, Germany*
116 *The Henryk Niewodniczanski Institute of Nuclear Physics, Polish Academy of Sciences, Cracow, Poland*
117 *The University of Texas at Austin, Austin, Texas, United States*
118 *Universidad Autónoma de Sinaloa, Culiacán, Mexico*
119 *Universidade de São Paulo (USP), São Paulo, Brazil*
120 *Universidade Estadual de Campinas (UNICAMP), Campinas, Brazil*
121 *Universidade Federal do ABC, Santo Andre, Brazil*
122 *University College of Southeast Norway, Tonsberg, Norway*
123 *University of Cape Town, Cape Town, South Africa*
124 *University of Houston, Houston, Texas, United States*
125 *University of Jyväskylä, Jyväskylä, Finland*
126 *University of Liverpool, Department of Physics Oliver Lodge Laboratory, Liverpool, United Kingdom*
127 *University of Tennessee, Knoxville, Tennessee, United States*
128 *University of the Witwatersrand, Johannesburg, South Africa*
129 *University of Tokyo, Tokyo, Japan*
130 *University of Tsukuba, Tsukuba, Japan*
131 *Université Clermont Auvergne, CNRS/IN2P3, LPC, Clermont-Ferrand, France*
132 *Université de Lyon, Université Lyon 1, CNRS/IN2P3, IPN-Lyon, Villeurbanne, Lyon, France*
133 *Université de Strasbourg, CNRS, IPHC UMR 7178, F-67000 Strasbourg, France, Strasbourg, France*
134 *Université Paris-Saclay Centre d'Études de Saclay (CEA), IRFU, Department de Physique Nucléaire (DPhN), Saclay, France*
135 *Università degli Studi di Foggia, Foggia, Italy*
136 *Università degli Studi di Pavia, Pavia, Italy*
137 *Università di Brescia, Brescia, Italy*
138 *V. Fock Institute for Physics, St. Petersburg State University, St. Petersburg, Russia*
139 *Variable Energy Cyclotron Centre, Kolkata, India*
140 *Warsaw University of Technology, Warsaw, Poland*
141 *Wayne State University, Detroit, Michigan, United States*
142 *Westfälische Wilhelms-Universität Münster, Institut für Kernphysik, Münster, Germany*
143 *Wigner Research Centre for Physics, Hungarian Academy of Sciences, Budapest, Hungary*
144 *Yale University, New Haven, Connecticut, United States*
145 *Yonsei University, Seoul, Republic of Korea*